AD_____

Award Number: DAMD17-03-1-0095

TITLE: Molecular Engineering of Vector-based Oncolytic and Imaging Approaches for Advanced Prostate Cancer

PRINCIPAL INVESTIGATOR: Lily Wu, M.D., Ph.D.

CONTRACTING ORGANIZATION: University of California
Los Angeles, Ca 90024

REPORT DATE: February 2006

TYPE OF REPORT: Annual

PREPARED FOR: U.S. Army Medical Research and Materiel Command
Fort Detrick, Maryland 21702-5012

REPORT DOCUMENTATION PAGE

Form Approved
OMB No. 0704-0188

1. REPORT DATE	2. REPORT TYPE	3. DATES COVERED
01-02-2006	Annual	1 Feb 2005 – 31 Jan 2006

4. TITLE AND SUBTITLE
Molecular Engineering of Vector-based Oncolytic and Imaging Approaches for Advanced Prostate Cancer

5a. CONTRACT NUMBER

5b. GRANT NUMBER
DAMD17-03-1-0095

5c. PROGRAM ELEMENT NUMBER

6. AUTHOR(S)
Lily Wu, M.D., Ph.D.

5d. PROJECT NUMBER

5e. TASK NUMBER

5f. WORK UNIT NUMBER

7. PERFORMING ORGANIZATION NAME(S) AND ADDRESS(ES)
University of California
Los Angeles, Ca 90024

8. PERFORMING ORGANIZATION REPORT NUMBER

9. SPONSORING / MONITORING AGENCY NAME(S) AND ADDRESS(ES)
U.S. Army Medical Research and Materiel Command
Fort Detrick, Maryland 21702-5012

10. SPONSOR/MONITOR'S ACRONYM(S)

11. SPONSOR/MONITOR'S REPORT NUMBER(S)

12. DISTRIBUTION / AVAILABILITY STATEMENT
Approved for Public Release; Distribution Unlimited

13. SUPPLEMENTARY NOTES
Original contains colored plates: ALL DTIC reproductions will be in black and white.

14. ABSTRACT Hormone refractory and metastatic prostate cancer are not well understood. Better animal models, diagnostic and treatment modalities are sorely needed for these advanced stages of disease. We have coupled non-invasive optical imaging to develop metastatic prostate cancer animal models, and vector-based diagnostic and therapeutic approaches. A highly potent and prostate-specific transcriptional regulatory system (TSTA) has been utilized to restrict the expression of our adenoviral vector specifically to prostate or prostate cancer cells. In the diagnostic approach, this TSTA system will be applied to express imaging reporter gene. Alternatively, the TSTA system will be applied to regulate the expression of viral replication proteins in the therapeutic approach. In doing so, the viral amplification and cell lysis will be directed in a prostate-specific manner. To date, the progress of this project is according to the proposed plan as the feasibility and the functionality of the prostate-targeted oncolytic system was demonstrated. Interestingly, during our investigation, we have developed several metastatic human prostate tumor models. The cancer dissemination process in these models can be easily monitored by non-invasive imaging. These metastatic animal models will be the bases for us to investigate the efficacy of our diagnostic and oncolytic therapeutic viral vectors.

15. SUBJECT TERMS
Prostate Cancer

16. SECURITY CLASSIFICATION OF:				18. NUMBER OF PAGES	19a. NAME OF RESPONSIBLE PERSON
					USAMRMC
a. REPORT	b. ABSTRACT	c. THIS PAGE			19b. TELEPHONE NUMBER *(include area code)*
U	U	U	UU	26	

Standard Form 298 (Rev. 8-98)
Prescribed by ANSI Std. Z39.18

Table of Contents

Introduction:
The scope of this project is to develop adenoviral vectors that are capable of mediating gene expression specifically in prostate and prostate cancer cells. We propose to incorporate a highly potent and specific two-step transcriptional amplification (TSTA) system to mediate prostate-targeted gene expression. In diagnostic applications, this targeted vector will be utilized to express optical and PET imaging reporter genes. The hypothesis is that administration of these imaging reporter vectors could detect prostate metastatic cells in living animals. In a second therapeutic approach, the TSTA system is employed to regulate viral replication, which leads to specific lysis of prostate tumor cells. Creation of consistent and easy to follow metastatic prostate cancer models will be very useful towards the evaluation of the proposed vector-based diagnostic and therapeutic approaches.

Body:
Task 1A: Determine sensitivity of vector-based imaging.
In the last year's annual report, we demonstrated that the prostate-targeted adenoviral vector (AdTSTA-sr39tk) can produce robust PET imaging signals in androgen-independent as well as androgen-dependent tumor models by utilizing tissue specific transcriptional amplification (TSTA) system. Two studies have been published from our group demonstrating the prostate-targeted imaging and therapeutic activity of AdTSTA-sr39tk (see below). Based on an earlier publication (Sato et al. Mol Ther 2003) we realized that the activity of the original head-to-head configured TSTA vector can be improved upon. To accomplish this goal, we took on several different approaches (see Figure 1). Instead of locating two components

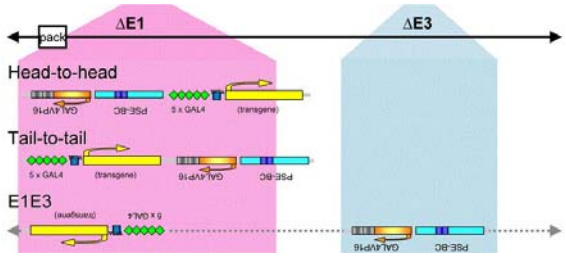

Figure 1. Additional configuration of the TSTA system in adenovirus. In addition to original configuration of the TSTA system (head-to-head), tail-to-tail and E1E3 constructs were created. To make tail-to-tail, both expression cassettes were inverted and inserted in E1 region. The E1E3 was constructed using the plasmid containing activator in E3 region.

(GAL4VP16 activator and reporter driven by GAL4 binding sites) of the TSTA system as 3' to 5'-5' to 3' (designated as head-to-head), we developed 5' to 3'-3' to 5' (named tail-to-tail) and one in E1 and another in E3 (named E1E3) (FIGURE 1). *In vitro* analysis suggested that the E1E3 vector has the higher androgen induction over both head-to-head and tail-to-tail vector (Figure 2A), and it also exhibited superior cell specificity assayed by activity in prostate cancer cell (LNCaP) over non-prostate cell line, HeLa (Figure 2B). Collectively, we are able to further improve TSTA vector, resulting in more robust activity (tail-to-tail, T-T), more androgen responsiveness (T-T and E1E3) and cell-specificity (E1E3) compared to the original (head to head, H-H) construct. The enhanced cell-selectivity of the E1E3 construct is particular pertinent to Task 2, as the designed configuration of our replicating oncolytic construct is similar to the E1E3 vector (see Figure 4).

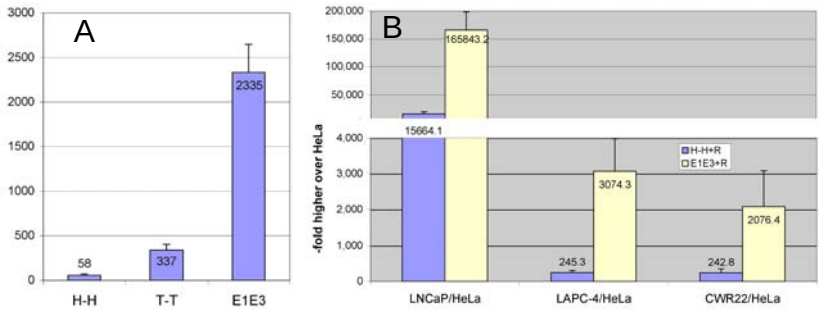

Figure 2. Improvements of the other configurations of the TSTA vectors. A. Tail-to-tail and E1E3 vectors showed superior androgen induction over head-to-head vector in LNCaP. B. In comparison to HeLa (negative cell line), the E1E3 vector exhibited higher specificity in all of prostate cell lines tested.

Task 1B: Optical imaging in preclinical models.
We have established prostate tumor models that consistently metastasize to regional lymph nodes and lung. As reported last year, these models were induced by expression of pro-

lymphangiogenic growth factors (VEGF-C and VEGF-C (C156S) mutant) in the tumor (see Figure 3). These models will greatly facilitate the evaluation of the diagnostic and therapeutic capabilities of our imaging and oncolytic vectors.

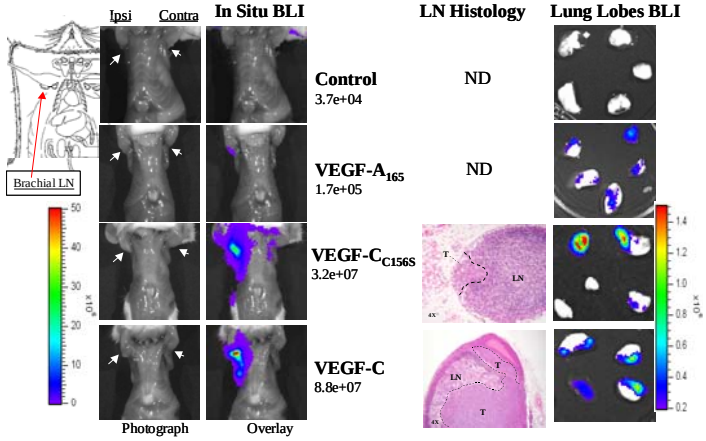

Figure 3. VEGF-C induces LN metastasis. LAPC-9 prostate tumors expressing designated vascular growth factors were grafted in right upper back. Expression of VEGF-C and C156S mutant resulted in metastasis to ipsilateral brachial node (arrow) and lung, confirmed by optical CCD imaging and histology. VEGF-A induces metastasis weakly.

Task 1C: Generation of gutless diagnostic Ad, testing in TRAMP model.
We have encounter difficulty in achieving the preset goals of this task for two reasons. 1) The production yield of gutless adenoviral vector is very low, with significant contamination of the helper virus, a first generation adenoviral vector. 2) In our experience, the first generation TSTA diagnostic PET imaging vector is efficient to produce and exhibit high and cell-selective activity (Figure 1 & 2). Thus, we decided to pursue the TSTA vector for further development (see publication listed), and clinical-grade TSTA vector is currently being produced by NCI RAID program for upcoming clinical investigation.

Task 2A: Generation of therapeutic oncolytic adenovirus.
In last year's annual report, we confirmed that bi-directional E1A and E1B expression in a plasmid construct and separate virus can confer prostate-specific viral replication. Thus, we initiated the construction of all-in-one TSTA oncolytic adenovirus to overcome the drawback of. The all-in-one TSTA oncolytic adenovirus has E1A and E1B in divergent orientation with centrally located GAL4 binding site repeats (0, 2 or 4) inserted in E1 region and the synthetic transactivator GAL4VP16 regulated by modified PSA promoter inserted in E3 region (Figure 4). As we shown in Task 1A, superior specificity can be expected with this E1E3 configuration, which should be helpful to safeguard nonspecific viral replication in non-prostate tissues. To accomplish this, we first modified pAdEasy-1 plasmid which encompass most of adenoviral genome except left end. We then inserted the activator component of the TSTA system, chimeric PSA promoter driving GAL4VP16 transactivator, resulted in pAdNUEZ. The all-in-one TSTA oncolytic adenovirus was constructed by the homologous recombination between pAdNUEZ and pShuttleG4E1, which has bidirectional E1A and E1B expression cassettes driven by GAL4 binding site repeats (0, 2, or 4).

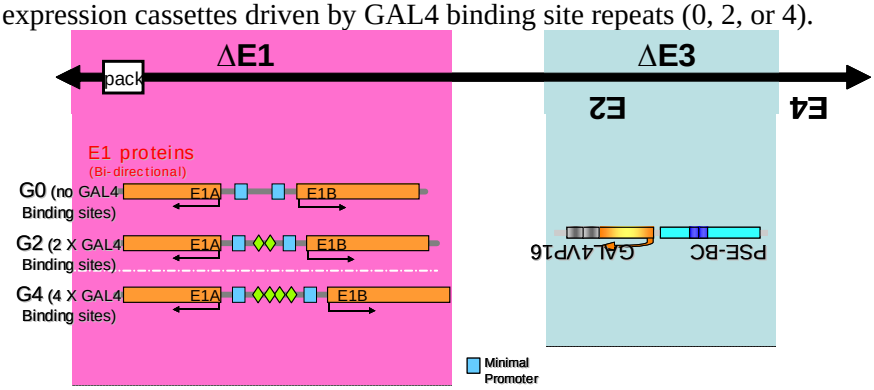

Figure 4. Schematic representation of the all-in-one TSTA oncolytic vectors. Gal4 binding sites, denoted by green diamonds, are situated centrally between divergently transcribed E1A and E1B. The G0 construct serves as a negative control.

Task 2B: In vitro evaluation of TSTA oncolytic adenovirus.

Prostate specific viral DNA replication was observed in *in vitro* infection study using the all-in-one TSTA oncolytic adenovirus with 4 repeats of GAL4 binding sites (AdG4A), which is expected to be the most efficient replicating construct (Figure 5).

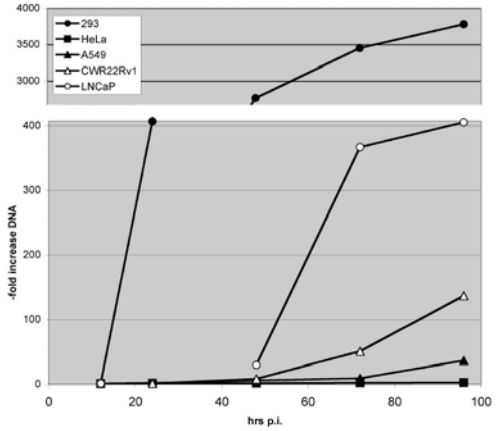

Figure 5. Prostate specific replication assessed by viral DNA of TSTA oncolytic adenovirus. Cell lines were infected with the all-in-one TSTA oncolytic adenovirus (AdG4A) and harvested at different time points until 4 days later. Total DNA was prepared from the each time points of the cell lines and subjected for real-time PCR analysis using the primer set for E2 region of adenovirus to quantify adenoviral DNA amplification. Negligible to low level of replication was seen in HeLa and A549. More than 100- and 400-fold increase of viral DNA was observed in CWR22Rv1 and LNCaP, respectively.

AdG4A exhibited significant viral DNA replication in LNCaP and CWR22Rv1, along with 293 as a positive control. The quantitative analysis of this study showed that 137- and 405-fold increase of viral DNA at 4 days compared to 12 hrs post infection in CWR22Rv1 and LNCaP, respectively. To further confirm the TSTA oncolytic viral replication, we infected prostate cancer cell lines, LNCaP and LAPC-4, and examined the expansion in infectious virus by plaque formation on 293 cells (Figure 6). All-in-one TSTA oncolytic adenovirus

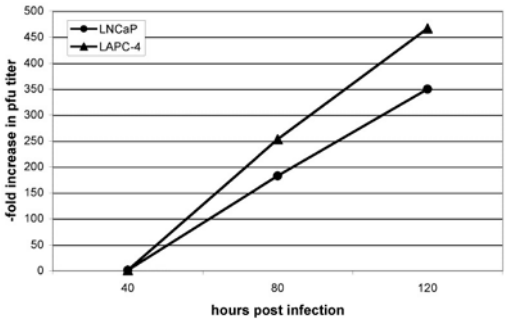

Figure 6. TSTA oncolytic viral replication in prostate cell lines. Two prostate cell lines, LNCaP and LAPC-4, were infected with AdG2A and harvested 40, 80 and 120 hrs after infection. Virus was extracted by repeating freezing and thawing three times. 293 cells were used to perform plaque formation. Fold increase in plaque forming unit at 80 and 120 hrs over 40 hrs are plotted.

with 2 GAL4 binding sites was used for this experiment. As shown in Figure 6, AdG2A showed efficient viral replication in both LNCaP and LAPC-4. This assay confirms that infectious virus is produced after the expansion of viral DNA. These preliminary findings indicate that the kinetics of viral replication appear to be delayed compared to wildtype virus or in 293 cells (Figure 5). The kinetics and efficiency of TSTA oncolytic adenovirus replication will be assessed in detail.

Task 3C: In vivo analyses of therapeutic activity of oncolytic virus.
After completing the generation of the oncolytic viruses and confirming their replicative activity, the immediate task will be assessed their therapeutic activity in preclinical prostate tumor models.

Key Research Accomplishments:

- We demonstrated that different configurations of prostate-specific TSTA adenoviral vector that exhibited superior specificity and androgen responsiveness than the original head-to-head configuration. This improved configuration has been incorporated into our oncolytic virus.
- We have developed lymphatic metastasis model of prostate cancer that can be monitored by molecular imaging. These models will be very useful in the development of vector-targeted diagnostic imaging.

- The all-in-one TSTA oncolytic adenovirus was constructed. Analyses in cell culture system showed promising results of replication of the virus in a robust and specific manner in prostate cancer cells.

Reportable Outcomes:

Manuscripts:

1) Sato M, Johnson M, Zhang L, Gambhir SS, Carey M, Wu L. Functionality of Androgen Receptor-based Gene Expression Imaging in Hormone Refractory Prostate Cancer. Clin Can Res 2005, 11:3743-9.

(This study confirms that modified PSA promoter (PSE-BC) mediated TSTA adenoviral vector can direct effective gene expression including PET imaging reporter gene in androgen-independent prostate tumor.)

2) Bao Y, Peng W, Verbitsky A, Chen J, Wu L, Rauen KA, Sawicki JA. Human coxsackie adenovirus receptor (CAR) expression in transgenic mouse prostate tumors enhances adenoviral delivery of genes. Prostate 2005, 64:401-7.

(This confirms that PSE-BC can direct prostate-specific expression in transgenic mouse model.)

3) Johnson M, Sato M, Burton J, Gambhir SS, Carey M, Wu L. MicroPET/CT monitoring of herpes thymidine kinase suicide gene therapy in a prostate cancer xenograft: the advantage of a cell-specific transcriptional targeting approach. 2005 Mol Imaging, 4:463-72.

(This study utilized TSTA adenovirus expressing HSV-tk gene in cytotoxic gene therapy that's coupled to molecular imaging.)

4) Bjorndahl MA, Cao R, Burton JB, Brakenhielm E, Religa P, Galter D, Wu L, Cao Y. Vascular Endothelial Growth Factor A Promotes Tumoral Lymphangiogenesis and Lymphatic Metastasis. 2005 Can Res, 65:9261-8.

(This study applied optical imaging to monitor lymphatic metastasis in a mouse model of fibrosarcoma.)

Abstracts:

1) Burton J.B., Brakenhielm E., Priceman S.J., Chavarria N., Alitalo K, and Wu L. Lymphatic And Systemic Metastasis Of Prostate Cancer Induce By VEGF-C. Inter-Prostate SPORE Meeting, Houston, Texas, Feb 4-6, 2006, invited speaker.
2) Figueiredo M.L.*, Sato M *, Chen M.N., Powell R, and Wu L. The Optimal Placement And Orientation Of The Bipartite Two-Step Transcription Amplification (TSTA) Expression System In Adenoviral Vectors For Prostate Cancer Gene Therapy. American Society of Gene Therapy (ASGT) annual meeting at Baltimore, MD. 6/2006
3) Sato M, Huyn S, Carey M, Gambhir SS, Wu L. Prostate targeted TSTA oncolytic adenovirus. American Society of Gene Therapy (ASGT) annual meeting at Baltimore, MD. 6/2006

Conclusions:

We have demonstrated that the TSTA approach can greatly augment prostate-specific gene expression, and the TSTA adenoviral vectors can mediate effective imaging and therapeutic activity in animal prostate tumor models. The lymphatic metastatic prostate cancer models we have developed will be applied to evaluate the diagnostic capability of our prostate-targeted TSTA imaging vectors. We also established the feasibility and functionality of prostate-specific oncolytic adenovirus regulated by the bi-directional TSTA method. The evaluation of our oncolytic therapeutic strategy in preclinical models of prostate cancer, including advanced androgen-independent and metastatic stage of disease, are underway.

Appendices:

Published work:

1) Sato M, Johnson M, Zhang L, Gambhir SS, Carey M, Wu L. Functionality of Androgen Receptor-based Gene Expression Imaging in Hormone Refractory Prostate Cancer. Clin Can Res 2005, 11:3743-9.
2) Johnson M, Sato M, Burton J, Gambhir SS, Carey M, Wu L. MicroPET/CT monitoring of herpes thymidine kinase suicide gene therapy in a prostate cancer xenograft: the advantage of a cell-specific transcriptional targeting approach. 2005 Mol Imaging, 4:463-72.

Functionality of Androgen Receptor–Based Gene Expression Imaging in Hormone Refractory Prostate Cancer

Makoto Sato,[1] Mai Johnson,[1,2] Liqun Zhang,[3] Sanjiv S. Gambhir,[4,5,6,7] Michael Carey,[3,5,6] and Lily Wu[1,4,5,6]

Abstract

Purpose: A highly augmented, prostate-specific two-step transcriptional amplification (TSTA) method was developed with the ultimate goal of delivering an effective and safe gene-based treatment to prostate cancer patients. Because very limited treatment options are available for recurrent hormone refractory prostate cancer (HRPC), it is imperative to assess whether the prostate-specific antigen (PSA) promoter-based TSTA gene therapy will be functional in HRPC.

Experimental Design: We tested the TSTA-driven adenovirus vector on three androgen-dependent and six HRPC models. Real-time gene expression was monitored by both optical imaging and the combined modality of positron emission tomography (PET) and computed tomography.

Results: The TSTA-driven firefly luciferase expressing adenoviral vector was active in all androgen receptor (AR)–expressing HRPC models, but inactive in AR- and PSA-negative lines. Interestingly, the TSTA-mediated gene expression was induced by hydrocortisone in MDA PCa 2b, a cell line with mutated AR that possesses altered ligand specificity. In animal models, the TSTA-mediated optical signal was more robust in the HRPC than androgen-dependent tumors. In a parallel trend, a TSTA vector that expresses the herpes simplex virus thymidine kinase PET reporter gene also displayed more robust PET signal in the HRPC tumor.

Conclusions: The activity of TSTA system is AR dependent and it recapitulates the functional status of endogenous AR. These data support the conclusion that AR function is activated in HRPC despite castrated levels of androgen. Together with the fact that majority of recurrent prostate cancers express AR and PSA, we foresee that the TSTA approach can be a promising gene therapy strategy for the advanced stages of prostate cancer.

Although recent data suggest that the death rate from prostate cancer is decreasing by 4% per year since 1994, it is still the second leading cause of cancer death in men, with an estimated 230,110 new cases and 29,900 deaths in the United States in 2004 (1). About one third of men with prostate cancer believed to have localized disease will already have micrometastasis at the time of therapy (2). Despite treatment with surgery, 20% to 30% of the patients will suffer from disease recurrence as defined by serum prostate-specific antigen (PSA) elevation (3, 4). In the aggressive, high-grade (Gleason 8-10) disease, majority of PSA recurrence is detected within 2 years after surgery with median survival of <3 years (3). Hormone therapy blocking androgen function can induce short-term remission, but the refractory disease eventually recurs (2). At this stage, the disease is defined as androgen-independent (AI) or hormone refractory prostate cancer (HRPC). The median survival for patients with metastatic HRPC is ~18 months, and systemic chemotherapy provides only a palliation of symptoms (5).

Androgen receptor (AR), the mediator of the physiologic effects of androgen (6), regulates the growth of normal and malignant prostate epithelial cells. Following the binding of the activating ligand dihydrotestosterone, AR translocates from the cytoplasm into the nucleus, binds directly to DNA recognition sites, and induces the expression of androgen-responsive genes, including *PSA*. A central issue in HRPC is to understand the role of AR in this stage of disease. Would AR function be obsolete under treatment where the activating ligand was depleted? Several mechanisms have indicated the continual involvement of AR in HRPC (reviewed in ref. 7), including (*a*) *AR* gene amplification and overexpression; (*b*) altered ligand specificity of AR (promiscuous AR); and (*c*) activation of AR through cross-talks with other AI pathways. The precise role of AR in clinical

Authors' Affiliations: Departments of [1]Urology, [2]Molecular Cellular and Integrative Physiology, [3]Biological Chemistry, and [4]Molecular and Medical Pharmacology; [5]Crump Institute for Molecular Imaging; and [6]Jonsson Comprehensive Cancer Center, David Geffen School of Medicine, University of California, Los Angeles, Los Angeles, California; and [7]Department of Radiology and the Bio-X Program, Stanford University, Stanford, California

Received 9/28/04; revised 12/7/04; accepted 12/14/04.

Grant support: Department of Defense grant DAMD17-03-1-0095 and NIH grant R01 CA101904 (L. Wu); Department of Defense grant DAMD PC 020177 (M. Carey); NIH grant R01 CA82214 and Small Animal Imaging Resource Program grant R24 CA92865 (S.S. Gambhir); an interdisciplinary grant from Jonsson Comprehensive Cancer Center (M. Carey, L. Wu, and S.S. Gambhir); and Department of Defense Congressionally Directed Medical Reseach Program postdoctoral fellowship, PC020531 (M. Sato).

The costs of publication of this article were defrayed in part by the payment of page charges. This article must therefore be hereby marked *advertisement* in accordance with 18 U.S.C. Section 1734 solely to indicate this fact.

Requests for reprints: Lily Wu, Department of Urology, University of California, Los Angeles, 675 Charles Young Drive South, Los Angeles, CA 90095-1738. Phone: 310-794-4390; Fax: 310-825-3027; E-mail: lwu@mednet.ucla.edu.

situations is not fully understood. However, given the fact that AR expression is documented in the majority of HRPC cases (8, 9) and that PSA remains the most reliable marker for recurrent, metastatic prostate cancer (10), it is highly probable that the gene regulatory activity of AR is functional in this setting.

Several PSA or probasin promoter-based gene therapy approaches have been developed (ref. 11; reviewed in ref. 12). However, thorough investigations questioning the functionality of these AR-dependent therapeutic strategies in HRPC have not been completed. The current report uses cell-based activity measurements and *in vivo* molecular imaging to show that a highly amplified PSA promoter-derived (two-step transcriptional amplification, TSTA) system is active in HRPC models. Noninvasive bioluminescence imaging and positron emission tomography (PET) illustrate that the prostate-specific TSTA gene expression vectors exhibit robust activity in HRPC as well as androgen-dependent (AD) tumors. We project that our vector-based gene therapy coupled to molecular imaging would be a promising therapeutic option to develop for treating patients with recurrent disease.

Materials and Methods

Adenovirus constructs. AdTSTA-FL was constructed as previously described (13, 14). The AdTSTA-sr39tk was constructed with the AdEasy system (15). The head-to-head orientation of activator (BCVP2) and reporter (SR39tk) in the single plasmid was constructed by replacing FL with SR39tk in PBCVP2G5-L (16). The BCVP2G5-sr39tk fragment generated by *Not*I and *Sal*I digestion of PBCVP2G5-sr39tk was inserted into pShuttle, which was used in bacterial recombination to generate the full-length virus. The virus was grown on 293 cells, purified on a CsCl gradient, and titered by plaque formation assays on 293 monolayers. The level of replication competent adenovirus contamination in the viral stocks was evaluated by plaque formation on A549 cells. No plaque was detected at 10^8-fold higher viral stock dilution compared with assays on 293 cells.

Prostate cell lines and luciferase activity assay. The human prostate cancer cell lines LNCaP, CWR22Rv1, DU145, and PC-3 were grown in RPMI 1640 supplemented with 10% fetal bovine serum. Iscove's modified DMEM was used for LAPC-4. MDA PCa 2b line obtained from American Type Culture Collection (Manassas, VA) was grown in BRFF-HPC1 (Athena Environmental Sciences, Baltimore, MD) supplemented with 20% fetal bovine serum. For AdTSTA-FL assays, the cultured cells were plated onto 24-well plates at 5×10^4 cells per well with phenol red–free RPMI 1640 supplemented with 10% charcoal-stripped fetal bovine serum. Cells were counted and infected at 1 plaque-forming unit per cell [multiplicity of infection (MOI) = 1]. At 48 hours postinfection, the cells were harvested and lysed in radioimmunoprecipitation assay buffer [1% NP40, 0.1% sodium deoxycholate, 150 mmol/L NaCl, 50 mmol/L Tris-HCl (pH 7.5), and 1 mmol/L phenylmethylsulfonyl fluoride]. Luciferase activity was measured according to the manufacturer's instructions (Promega, Madison, WI) using a luminometer (Berthold Detection Systems, Pforzheim, Germany). Each value was normalized with protein concentration and calculated as the average of triplicate samples. The infectivity of all cell lines was assessed by quantitative PCR of internalized viral DNA and expression mediated by constitutive AdCMV-FL as previously described (14). Relative to the infectivity of LNCaP cells (designated as 1), the infectivity of all other lines are within 2-fold. The highest infectivity was in CWR22rv1 (2.0) and the lowest was in PC-3 (0.7). Due to the similarity of infectivity among the cell lines, activity results reported here were not adjusted.

Synthetic androgen methylenetrienolone (R1881; NEN Life Science Products, Boston, MA) or the antiandrogen bicalutamide (casodex) was added to experiments as indicated. To measure the androgen induction effect, we used the activity in the presence of 10 μmol/L bicalutamide as the basal level rather than in charcoal-stripped fetal bovine serum. The TSTA system is highly amplified and low level of residual androgen in charcoal-stripped fetal bovine serum can activate expression (16). For Western analysis, cell lysates were fractionated on 4% to 20% gradient acrylamide gels (Bio-Rad, Hercules, CA) and subjected to immunoblot analysis with anti-AR N-20 (Santa Cruz Biotechnologies, Santa Cruz, CA) or β-actin A5316 (Sigma, St. Louis, MO) antibodies, and visualized with HRP-labeled secondary antibody and ECL (Amersham, Piscataway, NJ).

Statistical analyses were done using the two-tailed Student's *t* test. For all analyses, $P < 0.01$ was considered statistically significant.

Preparation of tumor cell suspension. Preparation of tumor cell suspensions was done by slight modification of a published protocol (17). Briefly, tumors were harvested, minced to 1 mm^3, and then incubated in 1% Pronase solution (Roche Molecular Biochemicals, Mannheim, Germany) for 20 minutes at room temperature. After overnight incubation in PrEGM media (Cambrex, Walkersville, MD) with Fungizone, the cultured cells were disaggregated by pipetting through sterile 200 μm Cell-Sieve mesh (Biodesign Inc. of New York, Carmel, NY). Tumor cells were infected at 1 plaque forming unit per viable cell (MOI = 1) and analyzed after 48 hours. No difference in the infectivity (determined by infection with a green fluorescent protein expressing adenoviral vector) or nonspecific viral toxicity was observed between the androgen-dependent and androgen-independent LAPC-9 tumor cells.

Thymidine kinase enzyme assay. LNCaP and LAPC-4 were plated onto six-well plates at 5×10^5 cells per well and infected with AdTSTA-sr39tk at MOI = 1. R1881 (10 nmol/L) or asodex (10 μmol/L) was added to the infected cells as indicated and the cells were harvested and lysed in 0.5% NP40, 25 mmol/L NaF, 3 mmol/L β-mercaptoethanol, and 10 mmol/L Tris-HCl (pH 7.0) after 48 hours. The protein concentration of the cell lysates was determined by the detergent-compatible protein assay (Bio-Rad); 1 μg of the lysate was mixed with 3 μL Tk mix ([^{3}H]penciclovir (Movarek Biochemicals, Brea, CA), 250 mmol/L Na_2HPO_4 (pH 6.0), 25 mmol/L ATP, and 25 mmol/L Mg acetate) and incubated at 37°C for 20 minutes. Reactions were terminated by the addition of 40 μL cold water and heating at 95°C for 2 minutes. Forty microliters of mixture was blotted onto DE81 filters (Whatman, Clifton, NJ). The filters were dried and washed thrice with 4 mmol/L ammonium formate and 10 μmol/L thymidine, once in water and twice in 95% ethanol. After drying, the filters were counted by scintillation. Each value was calculated as the average of duplicate samples.

Animal experiments with optical and positron emission tomography imaging. Animal care and procedures were done in accordance with the University of California Animal Research Committee guidelines. Ten- to twelve-week-old male SCID mice obtained from Taconic Farms (Germantown, NY) were implanted s.c. with a tumor chunk (~0.2 cm diameter) coated with Matrigel (Collaborative Research, Bedford, MA) and allowed to grow to ~0.8 cm diameter (18). For the optical imaging experiments, 10^7 plaque-forming units of AdTSTA-FL were subdivided and injected intratumorally (i.t.) into three sites. *In vivo* expression was monitored sequentially using a cooled IVIS CCD camera (Xenogen, Alameda, CA). For each imaging session, the mice were anesthetized with ketamine/xylazine (4:1), given the D-luciferin substrate (200 μL of 150 mg/kg substrate in PBS) i.p., and imaged after a 20-minute incubation. Images were analyzed with IGOR-PRO Living Image Software as described (13, 19). Immunohistochemistry to detect AR expression in the tumor was done with anti-AR antibody (Upstate, Co., Charlottesville, VA) as previously described (13, 19).

For micro-PET imaging, 10^9 plaque-forming units (~30 μL) of AdTSTA-sr39tk were injected i.t. for 4 consecutive days. PET imaging was done on day 7 using ~200 μCi [^{18}F]FHBG substrate (specific activity 5-10 Ci/mmol) that was administered via the tail vein. After 1 hour of uptake time, mice were given inhalation isoflurane anesthesia, placed in a prone position, and imaged for 20 minutes in the micro-PET scanner (Concorde Microsystems, Knoxville, TN).

Images were reconstructed using a filtered back projection reconstruction algorithm. Micro–computed tomography (micro-CT; Imtek, Inc., Knoxville, TN) was done for the same animal sequentially, and images were overlapped using ASIPro VM (Concorde Microsystems).

Results

The transcriptional amplification activity in prostate cancer cell lines. We have developed several transcriptionally targeted gene expression systems based on the PSA gene regulatory regions. The method that exhibits most potent activity, tissue selectivity, and androgen regulation is termed two-step transcriptional activation. It uses an enhanced PSA promoter (20) that drives a potent GAL4VP16 synthetic activator, which in turn binds to tandem repeats of GAL4 binding sites to activate the secondary reporter or therapeutic gene. This TSTA method achieved nearly 1,000-fold augmentation of activity over the native PSA promoter and is more active than the strong viral cytomegalovirus promoter (14). Recently, we have shown that AR in hormone refractory LAPC-9 tumors is functionally active, and it binds to known sites in the PSA gene regulatory region by chromatin immunoprecipitation (13). Expanding upon this observation, the key objective of this study is to survey the activity of TSTA vectors in a wider array of HRPC models and to visualize the *in vivo* activity of the vectors by multimodal molecular imaging techniques.

The activity of the TSTA adenoviral vector (AdTSTA-FL; Fig. 1A) was first determined in two AD lines LNCaP and LAPC-4, and three HRPC lines CWR22Rv1, DU145, and PC-3. As shown in Fig. 1B, AdTSTA-FL activity was negligible in the AR-negative DU145 and PC-3 lines. In the three AR-expressing lines, the activity of AdTSTA-FL was stimulated by androgen ranging from 11.4- to 60.6-fold. When bicalutamide (10 μmol/L) was given simultaneously in the presence of synthetic androgen R1881 (10 nmol/L), a ~50% suppression of peak activity was observed (data not shown). In the presence of androgen, LNCaP cells exhibited the highest expression at 4.8 times the level of LAPC-4 and 14.4 fold-higher than CWR22Rv1.

We also investigated the activation in a fourth HRPC line, MDA PCa 2b, which interestingly expresses AR with a double mutation (L701H and T877A) that allows gene expression and growth to become glucocorticoid responsive (21). As shown in Fig. 1C, gene expression mediated by this promiscuous AR responded to both androgen and hydrocortisone. The induction was 105-fold by hydrocortisone and 144-fold by R1881. The absolute expression level in MDA PCa 2b was 4.4-fold lower than CWR22Rv1. Based on these expression data, we deduced that the PSA-based TSTA method is active in HRPC but its activity is dictated by the AR function in the cell.

Two-step transcriptional amplification activity in hormone refractory LAPC-9 tumor monitored by optical imaging. LAPC-9 and LAPC-4 are two human prostate tumors that can recapitulate the clinical scenario of HRPC (17, 18). They grow routinely in intact male mice and undergo tumor regression upon castration. However, after a substantial time delay, a hormone refractory tumor develops, mimicking the recurrence of HRPC. The activity of AdTSTA-FL was monitored by optical imaging of paired AD and hormone refractory LAPC-9 tumors from days 4 to 14 (Fig. 2A). By this real-time *in vivo* activity measurement, hormone refractory tumors supported a higher level of transgene expression than AD tumors. Immunohistochemistry analysis revealed that the AR protein was expressed in both AD and HRPC tumors, but the magnitude of expression is very heterogenous among the tumor cells (Fig. 2B).

Equivalent gene delivery into the different tumors by i.t. viral injection was difficult to achieve. Thus, we converted the paired tumors into single cell suspension to examine androgen regulation and the activity of the TSTA system more accurately. In doing so, the dosage of viral vector and androgen administered on a per cell basis can be controlled. The dispersed tumor cells were infected with AdTSTA-FL in the

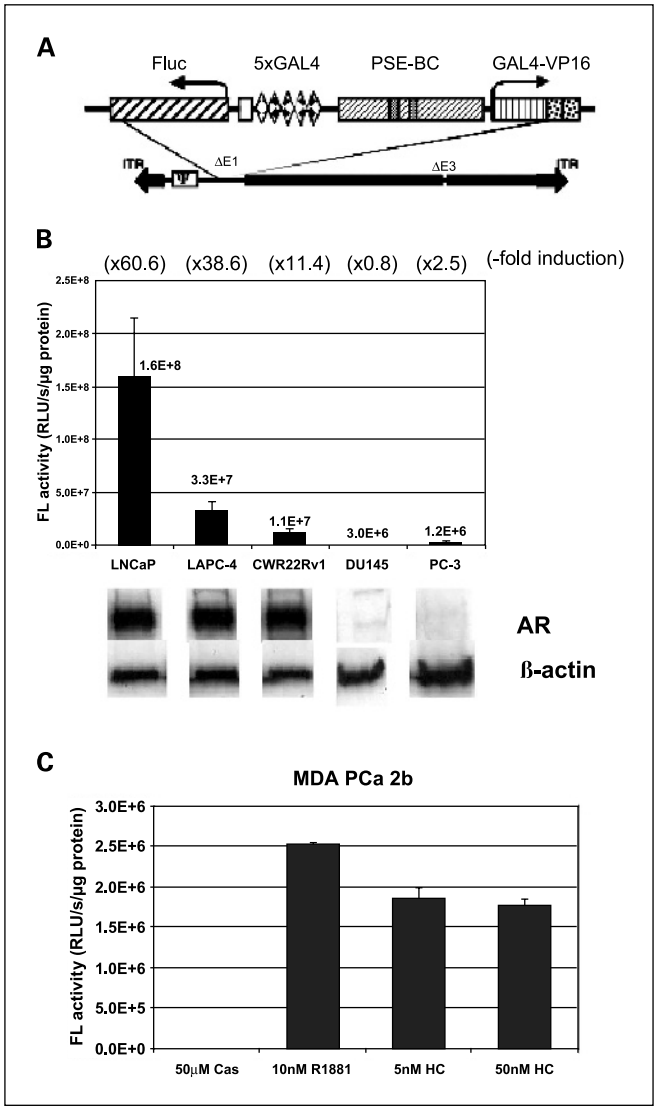

Fig. 1. The activity of AdTSTA-FL and the induction with androgen in a panel of prostate cancer cell lines. *A,* schematic representation of the AdTSTA-FL. The two TSTA components of activator (*GAL4-VP16* driven by *PSE-BC*) and reporter (*Fluc* driven by *5xGAL4*) are inserted into E1 region of recombinant adenovirus. *B,* AdTSTA-FL activity on a panel of prostate cancer cell lines. The cell lysates were harvested 2 days after infection and subjected to FL activity and Western analysis with anti-AR antibody. Fold inductions calculated by the activity ratio with 10 nmol/L R1881 over 10 μmol/L casodex are indicated at the top in parentheses. The activity difference between the AR-positive cell lines and the AR-negative lines (*DU-145* and *PC-3*) is statistically significant ($P < 0.01$). *C,* AdTSTA-FL activity in MDA PCa 2b. The cells were infected and incubated with 10 μmol/L casodex, 10 nmol/L R1881, and 5 and 50 nmol/L hydrocortisone.

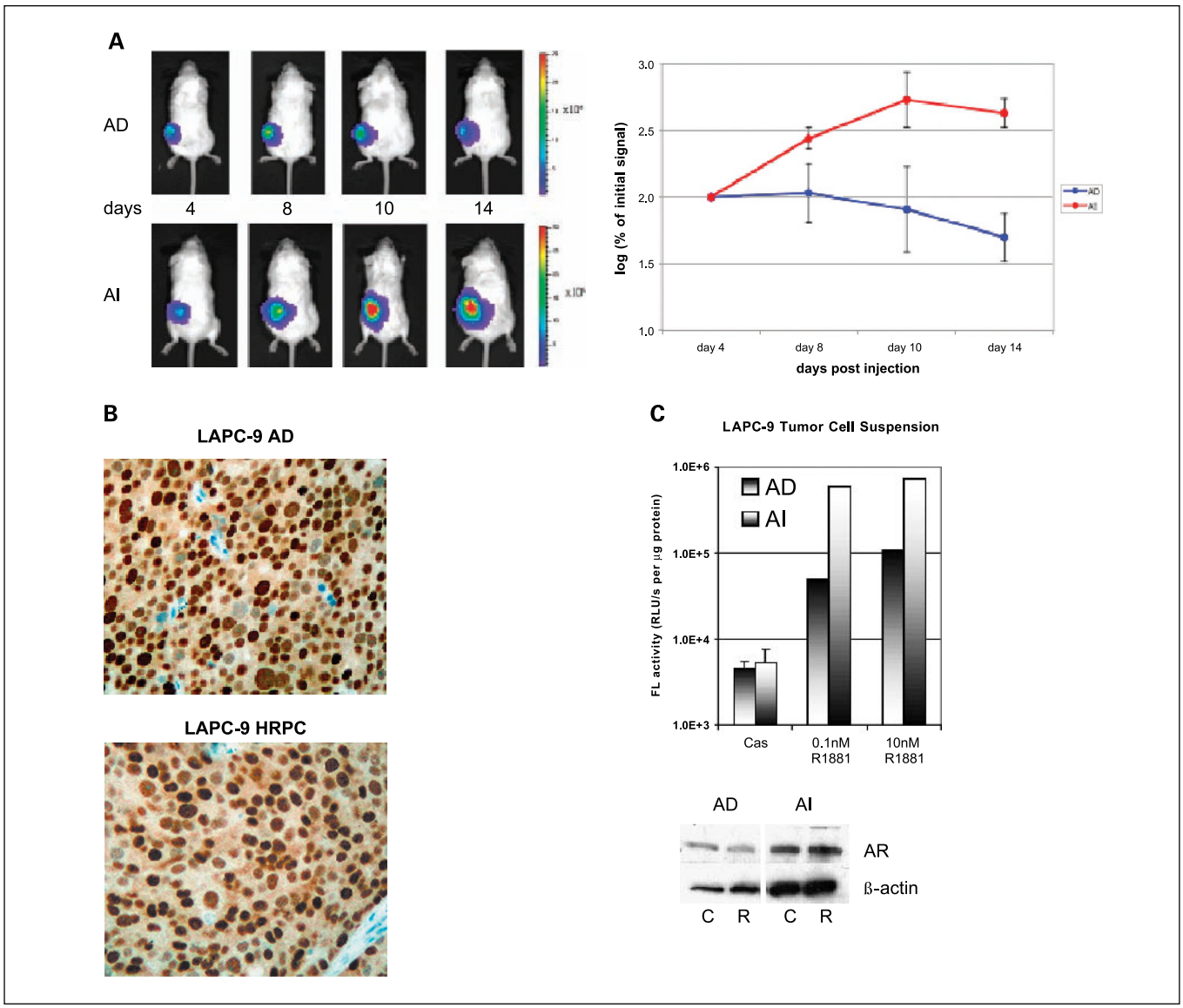

Fig. 2. AdTSTA-FL – mediated activity *in vivo*. *A,* AdTSTA-FL – mediated optical signal in LAPC-9 AD and AI (HRPC) tumors. Ten million infectious units of virus were injected i.t. and imaged by optical CCD camera on the specified day postviral injection. Common logarithms of the percentages of the signal at day 4 of AD and AI tumors are plotted in the right panel. *B,* AR protein in LAPC-9 tumors. Paraffin-fixed, thin tumor sections were stained with anti-AR antibody. *C,* AdTSTA-FL activity in tumor cell suspension prepared from LAPC-9 AD and AI (HRPC) tumors. Tumor cell suspension was infected with AdTSTA-FL at MOI = 1 and incubated in the presence of 10 μmol/L casodex or 0.1 or 10 nmol/L R1881. The cell lysates were prepared after 2 days and subjected to FL assay and AR Western blot [10 μmol/L casodex (*C*); 10 nmol/L R1881 (*R*)]. The activity difference between AI and AD cells in the presence of R1881 was statistically significant ($P < 0.01$).

presence of specified ligands. AR protein and androgen-responsive FL activity was observed in both cell populations (Fig. 2C). In close agreement with the optical imaging results in tumors, we also observed that the activity of AdTSTA-FL is 7.2-fold higher in the hormone refractory (AI) than in AD tumor cells in culture in the presence of ≥1 nmol/L concentrations of R1881.

Use of the two-step transcriptional amplification vector in positron emission tomography imaging. It is important to develop molecular imaging approaches that can be applied in clinical settings for advanced prostate cancer. To this end, we adapted our prostate-specific gene imaging to PET, a radionuclide functional imaging modality that enables three-dimensional signal localization. An adenoviral vector that expresses the herpes simplex virus thymidine kinase (*HSV-tk*) PET reporter gene under the control of TSTA was generated (Fig. 3A). An enhanced HSV-tk variant, sr39tk, was incorporated into the AdTSTA-sr39tk because this variant *tk* gene augments the uptake of radiolabeled PET tracers and improves PET imaging sensitivity by 2-fold (22). The sr39tk protein expression and enzymatic activity mediated by the vector was regulated by androgen (Fig. 3B and C).

AdTSTA-sr39tk was administered into AD and hormone refractory LAPC-4 tumors, and its activity was documented by the combined micro-PET/micro-CT. This combined imaging modality enables the precise localization of the PET signals with the anatomic information obtained from the CT scan. Using [^{18}F]FHBG as the PET substrate, robust signals were

observed in both AD and hormone refractory LAPC-4 tumors (Fig. 3D). The activity was higher in the hormone refractory tumor (0.78% injected dose/g) than in the AD tumor (0.50% injected dose/g). These results confirm that the TSTA-mediated prostate-specific gene imaging is feasible for advanced stages of tumor using the clinically relevant PET.

Discussion

Effective treatment options for recurrent prostate cancer are notably limited. Our goal has been to develop novel gene-based diagnostic and therapeutic approaches to treat advanced stages of prostate cancer. Toward this end, the well-studied PSA promoter/enhancer was utilized to achieve prostate-specific gene expression. Given that transcriptional regulation of the PSA promoter/enhancer is AR dependent, it was prudent to first verify that our PSA promoter-based expression strategy is feasible in HRPC. In this study, we showed that the highly amplified prostate-specific TSTA gene delivery vectors are indeed functional in many models of HRPC under androgen-deprived conditions.

Our data support that the presence of functional AR is necessary to activate PSA-based promoter constructs. However, other factors are likely to modulate AR activity in HRPC cells. The 14-fold range of luciferase activity observed in different models does not correlate with the level of AR expression or the status of AR mutation in the cell lines. The AR in LAPC-4 is wild type, whereas it contains the T877A mutation in LNCaP and the H874Y mutation in the ligand-binding

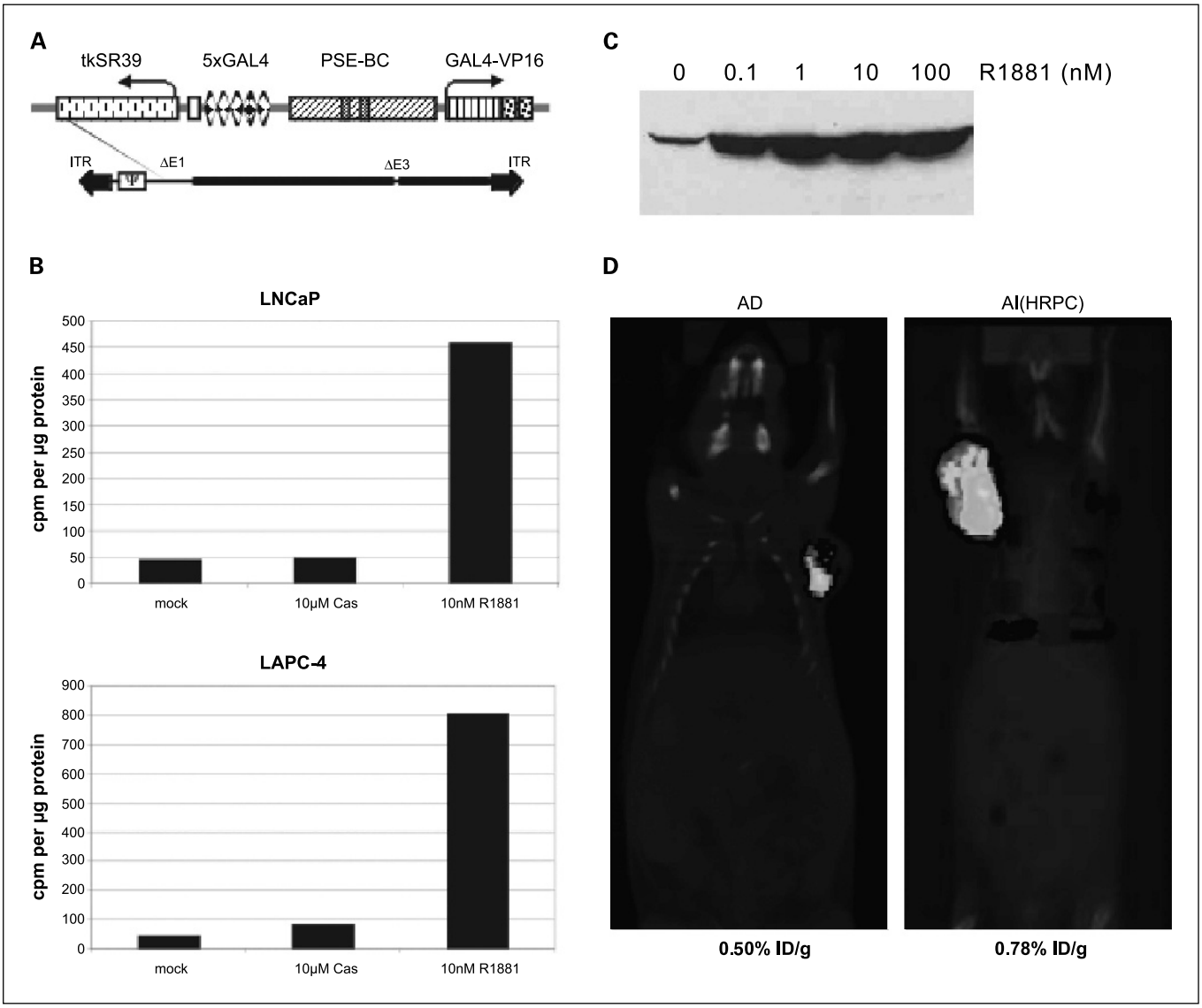

Fig. 3. The activity of AdTSTA-sr39tk and its application in micro-PET. *A,* schematic representation of the AdTSTA-sr39tk. The *sr39tk* gene is a HSV-tk variant with higher affinity for acycloguanosines. *B,* AdTSTA-sr39tk activity in AD prostate cancer cell lines LNCaP and LAPC-4. The cells were infected with AdTSTA-sr39tk at MOI = 1 and harvested 2 days later. The cell lysates were subjected to thymidine kinase enzyme assay. Phosphorylated forms of [^{3}H]penciclovir were counted and plotted after normalization with total cellular protein. *C,* androgen regulation of expression from AdTSTA-sr39tk. LNCaP cells were infected with AdTSTA-sr39tk at MOI = 5 and incubated with 0 to 100 nmol/L R1881. Cells were lysed and subjected to Western analysis using anti-HSV-tk polyclonal antibody. *D,* combined micro-PET and micro-CT of LAPC-4 AD and AI tumor. AdTSTA-sr39tk (4×10^9 infectious units) was injected to AD and AI LAPC-4 tumors. One week later, [^{18}F]FHBG injected animals were anesthetized and scanned for micro-PET and micro-CT sequentially. The signal in the tumor was measured by percentage injected dose of substrate per gram of tissue (*%ID/g*) listed below the image.

domain of CWR22Rv1. Differential activity of coactivators of the AR pathway could modulate AR function *in vivo*. Gregory et al. (23) reported elevated level of nuclear receptor coactivators, SRC1, and SRC2 in recurrent prostate cancer. Recently, Dr. Tindall's group also showed that coactivator p300 confers increased growth and progression potential in prostate cancer (24). Many other growth signaling pathways, such as IGF, Her2, or IL6, can also modulate AR-mediated expression (reviewed in ref. 7). Further investigations are needed to determine the precise AR activation mechanism in different cases of HRPC.

Both optical imaging and PET illustrated higher TSTA activity in the hormone refractory xenograft subline versus the parental AD tumor in two models. These findings endorse the idea that activation of AR function occurs despite the castrated level of androgen *in vivo*. A recent report by Chen et al. (25) showed that 3- to 5-fold elevated expression of AR is a cardinal distinguishing feature between paired AD and hormone refractory tumors. Their work also supports that AR overexpression can lead to HRPC. In fact, the two models reported here were assessed in the gene expression profiling study (25). Moreover, our results showed that the real-time assessment of AR functional activity in prostate tumors, including HRPC, can be accomplished by introducing TSTA adenoviral vectors into the tumor.

In contemplating future applications in clinical settings, we postulate that the TSTA gene expression strategy will be active in all PSA-positive prostate cancers, which include the recurrent metastatic disease. Previous histologic evaluations of clinical materials have detected AR and PSA expression in all stages of prostate cancer (8, 26, 27). Recent preliminary results (reported at Specialized Programs of Research Excellence meeting July 2004, Baltimore MD) indicated that AR expression is detected in metastatic lesions, albeit at heterogeneous level. A subtype of HRPC, the neuroendocrine prostate cancer, lacks AR and is associated with poor prognosis (28, 29). We anticipate any AR-dependent gene expression approach will be inactive in neuroendocrine tumor cells. However, solitary neuroendocrine tumors are rare as most neuroendocrine tumor cells exist in small foci interspersed within conventional AR- and PSA-positive prostate adenocarcinoma. If an AR-dependent toxic gene therapy was applied to a mixed lesion, then indirect tumoricidal effects can be transmitted to neuroendocrine tumor cells via conventional prostate cancer cells by bystander effects (12).

Linking molecular imaging to gene therapy is a favorable method to assess the performance of the intended treatment. In an earlier study, visualization of distant metastases of prostate tumor was accomplished by optical imaging mediated through the use of a modified PSA promoter-based adenoviral vector (19). Due to the inability of light energy to penetrate deep into tissues, bioluminescence imaging is not applicable in humans. Thus, to translate the above-mentioned promising findings to the clinics, the application of a high-energy clinically relevant modality, such as PET, is needed. However, the HSV-tk–based PET imaging is several orders of magnitude less sensitive than optical imaging in small animal studies (30). The nearly three-order gain in activity of TSTA over native PSA promoter is a key factor to achieve the successful PET imaging of HRPC. Because the same principles are at work in animal micro-PET as in clinical PET, this result supports the idea of an equivalent gene-based approach in clinical studies.

Many studies have shown that the *sr39tk* gene can function effectively both as a PET reporter gene as well as a toxic suicide gene (12, 31). Recently, the AdTSTA-sr39tk was applied in a "one-two punch" imaging and suicide gene therapy to treat prostate tumor.[8] Compared to a constitutive cytomegalovirus-driven vector, the prostate-targeted TSTA vector not only elicited equivalent tumoricidal effects but also dramatically reduced systemic liver toxicity. The PET imaging correlated entirely with the therapeutic outcomes. These results indicate that the TSTA methodology is a promising platform to build gene-based diagnostic and therapeutic approaches to manage HRPC.

Acknowledgments

We thank W. Ladno, J. Edwards, and Dr. D. Stout for their skillful assistance in PET/CT imaging; Baohui Zhang for technical assistance; Giri Sulur for assistance on manuscript preparation; and Drs. David Agus (Department of Molecular and Medical Pharmacology, UCLA, Los Angeles, CA) and Margaret Black (Pharmaceutical Sciences, Washington State University, Pullman, WA) for the kind gifts of CWR22Rv1 cell line and polyclonal anti-tk antibody, respectively.

[8] Johnson et al., submitted for publication.

References

1. Weir HK, Thun MJ, Hankey BF, et al. Annual report to the nation on the status of cancer, 1975-2000, featuring the uses of surveillance data for cancer prevention and control. J Natl Cancer Inst 2003;95:1276–99.
2. Dowling AJ, Tannock IF. Systemic treatment for prostate cancer. Cancer Treat Rev 1998;24:283–301.
3. Pound CR, Partin AW, Eisenberger MA, Chan DW, Pearson JD, Walsh PC. Natural history of progression after PSA elevation following radical prostatectomy. JAMA 1999;281:1591–7.
4. Roehl KA, Han M, Ramos CG, Antenor JA, Catalona WJ. Cancer progression and survival rates following anatomical radical retropubic prostatectomy in 3,478 consecutive patients: long-term results. J Urol 2004; 172:910–4.
5. Tannock IF, de Wit R, Berry WR, et al; TAX 327 Investigators. Docetaxel plus prednisone or mitoxantrone plus prednisone for advanced prostate cancer. N Engl J Med 2004;351:1502–12.
6. Gelmann EP. Molecular biology of the androgen receptor. J Clin Oncol 2002;20:3001–15.
7. Feldman BJ, Feldman D. The development of androgen-independent prostate cancer. Nat Rev Cancer 2001;1:34–45.
8. Hobisch A, Culig Z, Radmayr C, et al. Distant metastases from prostatic carcinoma express androgen receptor protein. Cancer Res 1995;55: 3068–72.
9. Magi-Galluzzi C, Xu X, Hlatky L, et al. Heterogeneity of androgen receptor content in advanced prostate cancer. Mod Pathol 1997;10:839–45.
10. Bok RA, Small EJ. Bloodborne biomolecular markers in prostate cancer development and progression. Nat Rev Cancer 2002;2:918–26.
11. DeWeese TL, van der Poel H, Li S, et al. A phase I trial of CV706, a replication-competent, PSA selective oncolytic adenovirus, for the treatment of locally recurrent prostate cancer following radiation therapy. Cancer Res 2001;61:7464–72.
12. Wu L, Sato M. Integrated, molecular engineering approaches to develop prostate cancer gene therapy. Curr Gene Ther 2003;3:452–67.
13. Zhang L, Johnson M, Le KH, et al. Interrogating androgen receptor function in recurrent prostate cancer. Cancer Res 2003;63:4552–60.
14. Sato M, Johnson M, Zhang L, et al. Optimization of adenoviral vectors to direct highly amplified prostate-specific expression for imaging and gene therapy. Mol Ther 2003;8:726–37.
15. He TC, Zhou S, da Costa LT, et al. A simplified system for generating recombinant adenoviruses. Proc Natl Acad Sci U S A 1998;95:2509–14.
16. Zhang L, Adams JY, Billick E, et al. Molecular engineering of a two-step transcription amplification (TSTA) system for transgene delivery in prostate cancer. Mol Ther 2002;5:223–32.
17. Craft N, Chhor C, Tran C, et al. Evidence for clonal outgrowth of androgen-independent prostate cancer cells from androgen-dependent tumors through a two-step process. Cancer Res 1999;59: 5030–6.
18. Klein KA, Reiter RE, Redula J, et al. Progression of metastatic human prostate cancer to androgen

independence in immunodeficient SCID mice. Nat Med 1997;3:402–8.

19. Adams JY, Johnson M, Sato M, et al. Visualization of advanced human prostate cancer lesions in living mice by a targeted gene transfer vector and optical imaging. Nat Med 2002;8:891–7.

20. Wu L, Matherly J, Smallwood A, et al. Chimeric PSA enhancers exhibit augmented activity in prostate cancer gene therapy vectors. Gene Ther 2001; 8:1416–26.

21. Zhao XY, Malloy PJ, Krishnan AV, et al. Glucocorticoids can promote androgen-independent growth of prostate cancer cells through a mutated androgen receptor. Nat Med 2000;6:703–6.

22. Gambhir SS, Bauer E, Black ME, et al. A mutant herpes simplex virus type 1 thymidine kinase reporter gene shows improved sensitivity for imaging reporter gene expression with positron emission tomography. Proc Natl Acad Sci U S A 2000;97: 2785–90.

23. Gregory CW, He B, Johnson RT, et al. A mechanism for androgen receptor-mediated prostate cancer recurrence after androgen deprivation therapy. Cancer Res 2001;61:4315–9.

24. Debes JD, Sebo TJ, Lohse CM, et al. p300 in prostate cancer proliferation and progression. Cancer Res 2003;63:7638–40.

25. Chen CD, Welsbie DS, Tran C, et al. Molecular determinants of resistance to antiandrogen therapy. Nat Med 2004;10:33–9.

26. Sweat SD, Pacelli A, Bergstralh EJ, Slezak JM, Bostwick DG. Androgen receptor expression in prostatic intraepithelial neoplasia and cancer. J Urol 1999; 161:1229–32.

27. Koivisto PA, Helin HJ. Androgen receptor gene amplification increases tissue PSA protein expression in hormone-refractory prostate carcinoma. J Pathol 1999;189:219–23.

28. Krijnen JL, Bogdanowicz JF, Seldenrijk CA, et al. The prognostic value of neuroendocrine differentiation in adenocarcinoma of the prostate in relation to progression of disease after endocrine therapy. J Urol 1997; 158:171–4.

29. di Sant'Agnese PA. Neuroendocrine differentiation in prostatic carcinoma: an update on recent developments. Ann Oncol 2001;12 Suppl 2:S135–40.

30. Ray P, Wu AM, Gambhir SS. Optical bioluminescence and positron emission tomography imaging of a novel fusion reporter gene in tumor xenografts of living mice. Cancer Res 2003;63:1160–5.

31. Pantuck AJ, Matherly J, Zisman A, et al. Optimizing prostate cancer suicide gene therapy using herpes simplex virus thymidine kinase active site variants. Hum Gene Ther 2002;13:777–89.

Micro-PET/CT Monitoring of Herpes Thymidine Kinase Suicide Gene Therapy in a Prostate Cancer Xenograft: The Advantage of a Cell-specific Transcriptional Targeting Approach

Mai Johnson[1,*], *Makoto Sato*[1,*], *Jeremy Burton*[1], *Sanjiv S. Gambhir*[1,2], *Michael Carey*[1], *and Lily Wu*[1]

[1]University of California Los Angeles, and [2]Stanford University, USA

Abstract

Cancer gene therapy based on tissue-restricted expression of cytotoxic gene should achieve superior therapeutic index over an unrestricted method. This study compared the therapeutic effects of a highly augmented, prostate-specific gene expression method to a strong constitutive promoter-driven approach. Molecular imaging was coupled to gene therapy to ascertain real-time therapeutic activity. The imaging reporter gene (luciferase) and the cytotoxic gene (herpes simplex thymidine kinase) were delivered by adenoviral vectors injected directly into human prostate tumors grafted in SCID mice. Serial bioluminescence imaging, positron emission tomography, and computed tomography revealed restriction of gene expression to the tumors when prostate-specific vector was employed. In contrast, administration of constitutive active vector resulted in strong signals in the liver. Liver serology, tissue histology, and frail condition of animals confirmed liver toxicity suffered by the constitutive active cohorts, whereas the prostate-targeted group was unaffected. The extent of tumor killing was analyzed by apoptotic staining and human prostate marker (prostate-specific antigen). Overall, the augmented prostate-specific expression system was superior to the constitutive approach in safeguarding against systemic toxicity, while achieving effective tumor killing. Integrating noninvasive imaging into cytotoxic gene therapy will provide a useful strategy to monitor gene expression and therapeutic efficacy in future clinical protocols. *Mol Imaging* (2005) **X,** 1–10.

Keywords: Prostate cancer, molecular imaging, suicide gene therapy, targeted gene expression, systemic toxicity, two-tiered amplification, adenoviral vector.

Introduction

Prostate cancer remains the second leading cause of cancer-related mortality in men in the United States. Recurrent and disseminated disease contributes to the majority of the estimated 29,089 deaths in 2004. No effective treatment currently exists for the advanced stage of human prostate cancer [1]. Hence, limitations of current therapeutic options demand the development of more effective detection and treatment methods. Gene therapy is a promising treatment because a great variety of growth inhibitory strategies can be implemented [2–5]. When used in combination, it could also augment therapeutic effects of conventional prostate cancer treatment. In particular, cytotoxic therapy employing the herpes simplex virus type 1 thymidine kinase (HSV1-tk) gene has been widely used in both experimental and clinical settings [6,7]. Despite promising therapeutic efficacy in preclinical models, the clinical benefit of this HSV1-tk suicide gene therapy is unrealized at this time. The lack of therapeutic success could be attributed to limited specificity, modest potency, inadequate gene delivery, and inability to monitor gene expression at the targeted site [8]. In this study, we aim to address these challenges to improve upon the current status of prostate cancer gene therapy.

The use of prostate-specific promoter to express therapeutic gene is likely to be advantageous over constitutive promoters in achieving cell-specific selectivity. In support of this concept, specific gene transfer and expression in distant prostate metastatic lesions was achieved by employing a modified prostate-specific antigen (PSA) gene promoter [9]. However, the weak activity of the native PSA promoter precludes efficient gene expression in prostate cancer therapeutic applications [10]. Several methods have been used to enhance the activity of the PSA promoter. By duplicating the upstream enhancer core of the PSA promoter, a 20-fold enhancement of activity over the parental construct was achieved [11,12]. In a second method, a two-step transcriptional amplification (TSTA) strategy was employed, which boosted the activity of the native PSA enhancer/promoter over 1000-fold, exceeding the activity level of the strong cytomegalovirus immediate early (CMV) promoter [13,14]. In the two-tiered TSTA system (Figure 1A), the PSA regulatory region was employed to express the potent synthetic transcription activator,

Corresponding author: Lily Wu, University of California Los Angeles, 675 Charles Young Drive S, Los Angeles, CA 90095; e-mail: LWu@mednet.ucla.edu.
*These authors contributed equally.
Received 15 April 2005; Received in revised form 11 May 2005; Accepted 12 May 2005.

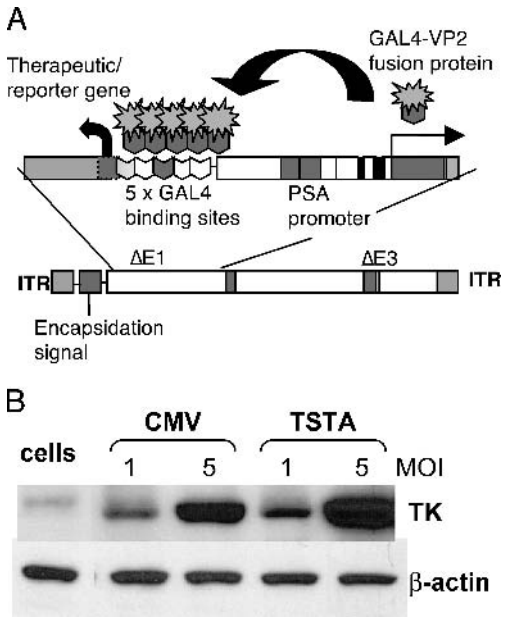

Figure 1. *Prostate-specific suicide gene therapy vector. (A) The Ad containing the TSTA system. The enhanced PSE-BC promoter drives the expression of the potent synthetic activator, composed of two herpes VP16 activation domains (aa 413–454) fused to the GAL4 DNA-binding domain (red). The GAL4-VP2 activators bind to the GAL4 binding sites, activating the expression of a therapeutic gene. These two components were inserted into an Ad5 vector. (B) The magnitude of sr39tk expression by AdTSTA-sr39tk. LNCaP cells were infected with AdCMV-sr39tk or AdTSTA-sr39tk at MOI 1 and 5. The level of sr39tk protein expression was assessed by Western blot using a polyclonal HSV1-tk antibody [15] as well as β-actin as a control.*

GAL4-VP2, which in turn activates the expression of a GAL4-responsive gene. The prostate cell specificity and androgen responsiveness activity of the PSA promoter were retained in the TSTA method [13–17].

Coupling molecular imaging approaches to gene therapy will allow real-time monitoring of in vivo gene delivery and expression [18]. Optical bioluminescent imaging based on the firefly luciferase gene has frequently been utilized to study gene expression in living animals [19–18,20,21]. Light is produced through the enzymatic interaction of luciferase with its substrate D-luciferin in the presence of magnesium and ATP [20]. The bioluminescence generated within the animal can be detected by a highly sensitive cooled charge-coupled device (CCD) camera [21,22]. This form of optical imaging is very rapid and inexpensive compared to radionuclide-based imaging. However, one advantage of radionuclide imaging is its ability to provide 3-D tomographic signals. Positron emission tomography (PET) is one such modality that has been adapted to studies in small animals, using the HSV1-tk or the enhanced sr39tk derivative as the reporter gene [18]. The sr39tk contained multiple amino acid substitutions at the active site, which greatly improved the binding affinity for guanosine analogues compared to the wild-type (WT) enzyme [23]. The use of the sr39tk gene has been demonstrated to increase the sensitivity of PET imaging by twofold over the WT HSV1-tk gene [24].

The unique enzymatic activity of HSV1-tk enables it to function both as a PET reporter gene as well as a cytotoxic suicide gene [15,24–26]. Unlike its mammalian counterpart, this HSV enzyme can efficiently phosphorylate guanosine analogues such as ganciclovir (GCV). The phosphorylation of various radioactive derivatives such as 9-(4-[^{18}F]-fluoro-3-hydroxymethylbutyl) guanine ([^{18}F]FHBG), will lead to the trapping and accumulation of the radiolabeled tracer in cells expressing HSV1-tk, which in turn can be detected and located by the PET scanner. The cytotoxic effects of HSV1-tk require the subsequent phosphorylation of the otherwise nontoxic GCV monophosphate by cellular kinases. The triphosphate derivative causes chain termination during DNA replication and can lead to chromosomal aberrations and cell death [25]. The pharmacologic dosage of GCV in cytotoxic therapy is three to four orders higher than the PET tracer dose. The sr39tk variant also exhibited stronger cytotoxicity compared to the WT enzyme [15]. The dual imaging and cytotoxic capability of the sr39tk gene is very useful in gene therapy, allowing researchers to directly monitor location, temporal representation, and magnitude of the therapeutic gene expression in vivo by noninvasive imaging.

In this study, we report the use of the bioluminescent optical CCD and micro-PET imaging to assess the effectiveness of TSTA-mediated gene therapy. Micro-PET imaging was utilized to monitor sr39tk expression by measuring the uptake of [^{18}F]FHBG in organs where the gene is expressed. More importantly, the tissue selectivity and high magnitude of the TSTA-mediated sr39tk suicide gene therapy resulted in diminished systemic side effects and effective antitumor activity in a human prostate cancer xenograft model.

Materials and Methods

Vector Design

The AdTSTA-sr39tk was constructed with the AdEasy system [27]. The head-to-head orientation of activator (BCVP2) and reporter (sr39tk) in the single plasmid was constructed by replacing FL with sr39tk in PBCVP2G5-L [13]. The BCVP2G5-sr39tk fragment generated by *Not*I and *Sal*I from PBCVP2G5-sr39tk was then ligated to pShuttle to generate pShuttleTSTA-sr39tk, which was used for the recombination with pAdEasy-1. The virus was propagated in 293 cells, purified on a CsCl gradient, and titrated by plaque assays on 293 cell monolayers.

Expression Analysis in vitro

Human prostate cancer cell line LNCaP was infected with AdCMV-sr39tk or AdTSTA-sr39tk at the multiplicity of one or five virus per cell. Cells were harvested 2 days after infection and lysed with RIPA buffer (0.1% Na deoxycholate, 0.1% SDS, 0.15M NaCl, 1mM EDTA, 10 mM Tris–HCl [pH 7.4] with protease inhibitor cocktail; Calbiochem, San Diego, CA). Equal amounts of total protein from each sample were subjected to SDS-PAGE. Following the transfer of analyzed proteins to PVDF membrane (Millipore, Bedford, MA), Western analysis was performed using polyclonal anti-HSV-tk antibody [15] and monoclonal anti-β-actin antibody [28]. Visualization was performed by BM Chemiluminescence (Roche Diagnostics, Indianapolis, IN) with HRP-conjugated respective antibodies.

Optical Imaging of Mice

Animal experiments were performed in accordance with the University of California Animal Research Committee guidelines. Ten to 12-week-old male SCID (Taconic Farms, Germantown, NY) mice were subcutaneously implanted with 0.2 cm tumor coated with matrigel. When tumors reached ~0.8 cm, the specified Ad was injected into the tumor for four consecutive days, using a 28G1/2 syringe (10 μL per site, at three different sites, and waiting 5 min between injections). Optical imaging was performed with an IVIS CCD camera (Xenogen, Alameda, CA). Mice were anesthetized with ketamine and xylazine (4:1), then given 200 μL of 15 mg/mL D-luciferin (Xenogen) intraperitoneally, and imaged 20 min after substrate administration.

Micro-PET/CT Imaging and GCV Treatment

For the therapeutic study, the specified sr39tk Ad was administered intratumorally at 1×10^9 pfu/day × 4 days (30 μL/day). On Days 8 and 22, animals were injected with 200 μCi [^{18}F]FHBG via the tail vein. Following an hour of substrate uptake, the entire animal was scanned for 20 min in a Focus micro-PET scanner (Concorde Microsystems, Knoxsville, TN) and transferred to a micro-CT scanner (MicroCAT I, Imtek, Knoxsville, TN), and imaged for 15 min at 50 keV, 325 μA, and 196 total angles of rotation in two bed positions. From Days 9 to 16, animals received intraperitoneal administration of GCV (80 mg/kg in 0.9 % saline) or saline vehicle. PET signals were quantified as the percentage of injected dose per gram (%ID/g) tissue. This %ID/g is a measure of the amount of tracer accumulated in a given area normalized to the injected amount and to the mass of the tissue examined. PET images were superimposed on CT images. All PET/CT data analyses and 3-D images were compiled using AMIDE. A total of six animals were used in each of four treatment groups. PET imaging was performed on four out of six animals in each group.

Quantitative PCR

Organs were frozen in liquid nitrogen, ground into fine powder, resuspended in 10 volumes lysis buffer (10 mM Tris–HCl pH 8.0, 5 mM EDTA pH 8.0, 200 mM NaCl, 0.2 % SDS, 100 μg/mL proteinase K), and incubated at 55°C for 3 hr. One milliliter of each lysate was treated with RNase A (50 μg/mL) for 20 min at 37°C, followed by extracting twice with phenol/chloroform/isoamyl alcohol (25:24:1). The DNA was precipitated and resuspended in TE buffer (pH 8.0). Real-time PCR was performed using the Opticon 2 Monitor (MJ Research, San Francisco, CA). The specific primers for β-actin and HSV-tk are: (β-actin: forward, 5′-TCA AGA TCA TTG CTC CTC CTG AGC-3′, reverse, 5′-TAC TCC TGC TTG CTG ATC CAC ATC-3′; HSV-TK: forward, 5′-ACA AAA AGC CAC GGA AGT CC-3′, reverse, 5′-AGT TGC GTG GTG GTG GTT T-3′). Primers for β-actin recognize an identical conserved region of the human and mouse gene. Reactions were run in triplicate, each containing 1× SYBR Green master mix (Applied Biosystems), 0.4 pmol/μL of primers and 100 ng genomic DNA in 25 μL. The amplification conditions were: 1 cycle of 2 min at 50°C and 1 cycle of 10 min at 95°C, followed by 35 cycles of 15 sec at 95°C, 30 sec at 60°C, and 30 sec at 72°C. After completion of PCR, 10 μL of the pooled triplicated reactions was run on a 2% agarose gel, resolving the 106 bp β-actin and 101 bp HSV-tk amplified fragment.

Immunohistochemical Analysis

Tumors harvested at Day 22 were fixed in 10% formalin overnight. Paraffin-embedded sections (4 μm) were deparaffinized, and stained with hematoxylin and eosin. Proliferating cells were visualized using mouse monoclonal Ki67 antibody 1:50 (Novocastra, Norwell, MA) at 4°C overnight. Color visualization of immunohistological reaction was performed with multilink antibody, streptavidin peroxidase (BioGenex, San Ramon, CA), and 3,3 diaminobenzidine (DAB) as previously described [12]. Apoptotic cells were visualized by using DeadEnd Colorimetric TUNEL System (Promega, Madison, WI), performed according to manufacturer's instructions. Samples were blinded and staining was quantified by dividing each tumor into four quadrants. Cells were then counted under ×40 magnification. Staining was recorded as a percentage of positive cells over total cells counted (average of 100 cells/field).

Liver Enzyme and PSA Assays

Blood was collected at various time points by the retro-orbital eye bleed method. Serum ALT levels were measured using GTP/ALT reagent strip with SPOTCHEM EZ system (HESKA, Fort Collins, CO). Serum PSA levels were measured in duplicates using PSA ELISA kit (American Qualex, San Clemente, CA). The relative rate of change in PSA was obtained by calculating the difference in PSA levels pre- and posttreatment divided by posttreatment.

Statistical Analysis

Statistical analyses were performed using the two-tailed Student's t test. For all analyses, $p < .05$ was considered statistically significant.

Results

Prostate-specific Gene Delivery Vector

Using the prostate-specific two-step TSTA method should be advantageous, as this method has been shown to boost the activity of a comparable one-step prostate-specific promoter by 50-fold [12,13,16]. In this study, the TSTA system was incorporated into an adenoviral vector to drive the sr39tk gene, which is designated as AdTSTA-sr39tk (Figure 1). The magnitude of sr39tk protein expression mediated by this prostate-targeted Ad was comparable to the AdCMV-sr39tk, as analyzed in LNCaP (Figure 1B) and LAPC-4 (data not shown) human prostate cancer lines. Furthermore, AdTSTA-sr39tk mediated gene expression was regulated by androgen and active in advanced AR+ androgen-independent prostate cancer cell lines and tumors [28]. The promising properties AdTSTA-sr39tk exhibited in cell culture studies lend support to assess its activities in preclinical prostate tumor models.

Imaging Transgene Expression in Prostate Tumors

To learn more about the in vivo activity of the gene therapy vectors, we applied several molecular imaging modalities, including bioluminescent imaging and micro-PET, to monitor transgene expression during treatment. The study design, as outlined in Figure 2A, was to compare the performance of the CMV versus the TSTA vectors. In the CMV group (i) of the first study, 4×10^8 infectious plaque forming units (pfu) each of the luciferase-expressing virus (AdCMV-FL) and the sr39tk-expressing virus (AdCMV-sr39tk) were coinjected into the tumor. The same viral dosage was used in the TSTA group (ii). Given that in both groups the luciferase and sr39tk are expressed from the same promoter and inserted into the same adenoviral backbone, the lucifer-

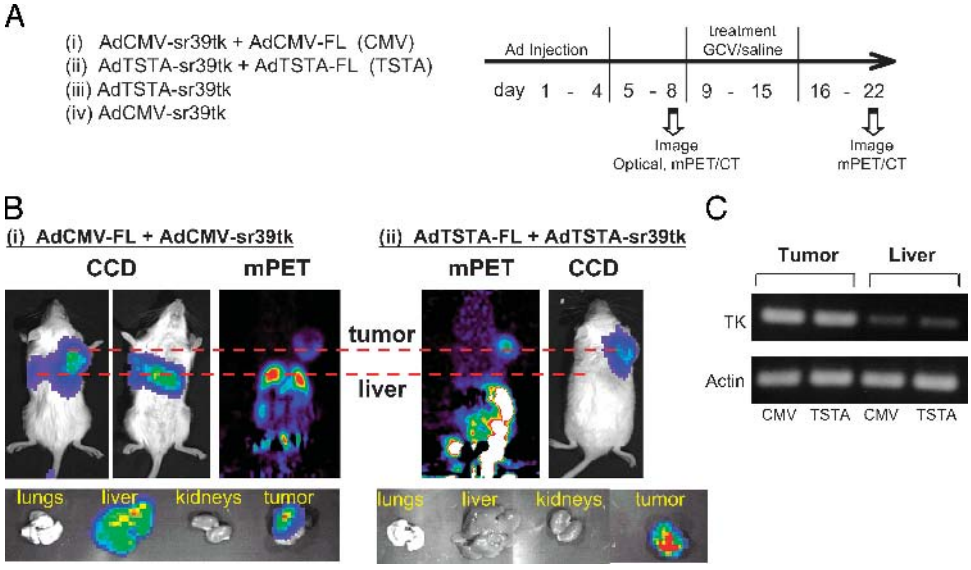

Figure 2. *Optical and PET imaging of vector mediated gene expression. (A) Therapeutic study scheme. Coinjection of the two vectors in groups i and ii in one study enables the optical FL signal to reflect the expression of sr39tk. Group iii and iv injections were performed in a second study to compare the therapeutic activity between the TSTA and the CMV vector. (B) Coinjection of the two adenoviral vectors (Ad) into LAPC-4 tumors. 4×10^8 pfu of each vector was injected and optical CCD imaging and micro-PET were performed on Day 8. Tumor and liver signals were detected in the CMV group (i), but in the TSTA group (ii) signals were limited to the tumors. Signals in the abdomen were due to the hepatobiliary and renal route of FHBG excretion. Animals were sacrificed at Day 22 and bioluminescent imaging of the isolated organs revealed the tumor-restricted expression of the TSTA vector. (C) PCR amplification of the sr39tk gene in the tumor and the liver. DNA was isolated from organs of AdCMV-sr39tk and AdTSTA-sr39tk treated animals (groups iii and iv). Real-time quantitative PCR was performed to quantify the sr39tk gene. Agarose gel resolution after completion of the 35-cycle PCR reaction revealed the presence specific HSV1-sr39tk DNA (101-bp amplified fragment) in the tumor and liver extracts. β-actin served as internal control.*

ase gene can serve as a reporter gene to reflect the expression of the sr39tk therapeutic gene. An advantage of this approach over a single vector expressing both imaging genes simultaneously is that the distribution and the gene expression profile can be verified by two independent vectors and imaging modalities. The LAPC-4 tumor was the model we examined. It is a PSA-expressing human prostate xenograft originally derived from a patient's lymph node metastases [29].

On Day 8, prominent optical signals were observed in the tumors of the CMV group (i). Strong signals emitted from the livers were consistently detected after intratumoral injection of CMV-driven vectors (Figure 2B, i). On the other hand, in the TSTA group (ii), the optical signal was confined to the tumor and the liver was devoid of signal (Figure 2B, ii). Similar to the optical analysis, micro-PET illustrated the same pattern of [^{18}F]FHBG uptake mediated by the sr39tk gene in the corresponding locations (Figure 2B).

To understand why gene expression was observed consistently in the liver of the CMV group but not in the TSTA group, real-time quantitative PCR was employed to quantify the viral distribution following intratumoral injection. The sr39tk gene delivered to the tumor relative to endogenous β-actin gene was 0.072 and 1.18 in a CMV and TSTA animal, respectively. In a CMV-treated animal, the ratio of the sr39tk gene delivered to the tumor was 452-fold higher than that in the liver. Similarly, the ratio in a TSTA-injected animal was 263-fold higher in the tumor than in the liver. The correct size of the sr39tk fragment was detected from the tumor and liver extracts (Figure 2C). These PCR data indicate that tumor-directed vector administration does not preclude gene delivery to nontargeted vital organs such as the liver. Our results would support the assumption that a tissue-specific vector provides added safety over a constitutively active vector. Imaging studies showed that the prostate-specific TSTA vector in the liver remained transcriptionally silent.

Treatment Side Effect Seen by Imaging

To compare the therapeutic activity between the CMV- and the TSTA-driven vector, a total of 4×10^9 pfu of the respective vector was injected into the LAPC-4 tumor (group iii and iv, Figure 2A). The animals were imaged by combined PET/CT on Day 8, just prior to GCV treatment (80 mg/kg for 7 days). The control groups received saline instead of GCV. All animals were re-imaged on Day 22, one week after the last day of GCV administration. At this point, no residual GCV should remain in the animal to interfere with uptake of PET substrate [^{18}F]FHBG. In the therapeutic studies, micro-CT was performed in series with the micro-PET. This combined technology enables the precise alignment of the PET signal with the anatomical location in the subject [30].

In the AdCMV-sr39tk injected group, a strong [^{18}F]FHBG PET signal was observed in the liver on Day 8 (Figure 3A). The [^{18}F]FHBG retention signal was not affected by saline treatment (2.5 ± 0.4 to 2.7 ± 0.06), but was decreased in the GCV-treated group from 3.7 ± 1.1 to 1.5 ± 0.3. The prominent [^{18}F]FHBG PET signal in the liver forecasted liver toxicity in this group. This is because the same sr39tk activity that phosphorylates [^{18}F]FHBG also functions in the first step of cytotoxic activation of GCV. After GCV treatment, a clear decrease of sr39tk-mediated PET signal in the liver was observed (Figure 3A, graph). The decrease in the functional PET signal could be attributed to the elimination of sr39tk expressing cell with GCV. No loss of PET signal was observed with saline treatment (Figure 3A, graph).

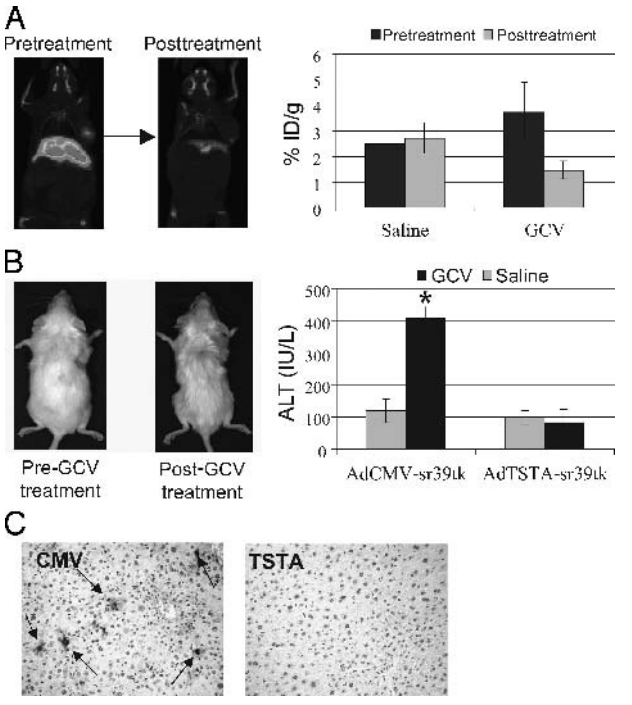

Figure 3. *Liver toxicity after GCV treatment in AdCMV-sr39tk animals. (A) Micro-PET/micro-CT of AdCMV-sr39tk treated animals. Compared to the saline treatment, GCV treatment (n = 6 per treatment group) resulted in a reduction of PET signal in the liver (PET, n = 4 per group). The graph on the right shows average [^{18}F]FHBG retention in the liver pre- and posttreatment. (B) Liver toxicity in the animals. GCV-treated mice in the CMV group were weak and disheveled. GCV treatment resulted in elevated serum ALT levels in the CMV group compared to TSTA and saline groups on Day 22. (C) Immunohistochemical analysis of the liver. Liver sections from these mice revealed significant TUNEL positive staining (arrows) indicative of apoptosis. This was not observed in the TSTA cohort.*

The extent of liver damage in the animals was assessed by several means including signs and symptoms of the animals, hepatic serology, and histology. Alanine aminotransferase (ALT) is an intracellular enzyme produced by hepatocytes that are released into the bloodstream as a result of liver cell destruction. The GCV-treated animals in the CMV group exhibited more than four times higher ALT than the saline control or TSTA groups (Figure 3B), and they appeared weak and unkempt. At the end point of the study, the average liver weight of the CMV group was 50% of the saline and TSTA-treated groups. Immunohistochemistry of the liver sections by terminal deoxynucleotidyl transferase (TdT)-mediated dUTP nick end labeling (TUNEL) revealed extensive apoptosis in the CMV GCV-treated animals (Figure 3B).

Monitoring Therapeutic Efficacy of Suicide Gene Therapy

The previous results (Figure 3) suggested that the destruction of sr39tk-expressing cells resulted in the diminution of sr39tk-mediated PET signals. Thus, we applied the radionuclide micro-PET/micro-CT to monitor the therapeutic effects of tumor cell destruction. In the AdTSTA-sr39tk-treated animals, PET signal in the tumor was significantly weakened on Day 22 compared with Day 8 (Figure 4A). Results of the entire TSTA treatment cohort showed that [^{18}F]FHBG accumulation in the tumors was 0.52 ± 0.04 %ID/g (n = 12) prior to GCV treatment on Day 8, 0.54 ± 0.09 %ID/g in the saline-treated group, and 0.33 ± 0.04 %ID/g in the GCV-treated group (n = 5) on Day 22. The GCV treatment resulted in a significant reduction of signals in the tumor (p = .026). Although adenoviral-mediated gene expression is expected to decay over time, we observed a higher magnitude of decrease (50%) in [^{18}F]FHBG retention in the GCV-treated group compared to a 20% decrease in saline-treated group from pre- to posttreatment (Figure 4A).

In the CMV treatment group, a decrease in PET signals was observed in the animal's tumor as well as in the liver following GCV treatment (Figure 3A). Three-dimensional reconstructed images of the whole animal were compiled from the PET/CT studies. The magnitude and localization of the PET signals pre- and post-GCV treatment are shown for one representative animal in the CMV and TSTA group (please refer to supplemental material for 3-D movie).

To validate the therapeutic outcome, PSA levels were examined during the course of treatment. Serum PSA, a widely used marker for the detection of prostate cancer, was applied to measure tumor load during suicide gene therapy. In this tumor model, serum PSA measurements have been shown to accurately reflect tumor volume and growth in several studies [29,31–33]. Serum PSA was sampled prior to treatment (baseline), and on Days 11 and 19 (i.e., 3 and 11 days post-GCV treatment). In the CMV group, the average baseline PSA was 21 ng/mL and increased to 26 ng/mL after GCV treatment, whereas the saline-treated group climbed to 72 ng/mL (p = .019). A similar trend was observed in the AdTSTA-sr39tk injected group. The average PSA in this cohort was 12 ng/mL at baseline and 13 ng/mL after GCV treatment compared with 46 ng/mL in saline controls (p = .018). The relative change of PSA was determined for each group (Figure 4B). The two saline-treated control groups showed continual tumor growth as is evident by the increasing PSA level, whereas tumor growth in the GCV-treated groups was halted.

Detailed histological examinations with hematoxylin and eosin (H&E) staining, proliferative marker Ki-67, and the apoptotic TUNEL staining were performed. Figure 4C shows representative tumor sections of eight different animals from the specified treatment groups. The hematoxylin dye (purple/blue) stains DNA content. Thus, the extent of purple/blue coloring in a tissue section is indicative of the extent of living cells. The overall hematoxylin staining in the unmagnified tumor sections of both saline groups was more extensive than the GCV-treated groups (Figure 4C). Moreover, the areas of proliferation that stained positive by Ki-67 were decreased in the GCV-treated tumors compared with saline controls. In contrast, the areas that did not stain for Ki-67 exhibited strong TUNEL staining. The apoptotic TUNEL staining also supports the PSA measurement that tumor growth was halted in the GCV-treated group. Quantitation of the tumor TUNEL staining revealed that an average of 67.6% tumor cells were positive in the GCV-treated versus 7.6% in the saline-treated tumor of the TSTA group. Overall, the histological assessment demonstrated that the GCV-treated tumors exhibited increased apoptosis (TUNEL staining), reduced proliferation (Ki-67 staining), and decreased living cells (hematoxylin staining). These observations therefore support that GCV treatment coupled to the sr39tk gene therapy results in effective tumor cell destruction.

Discussion

Achieving both potent and cell-selective expression could improve the therapeutic outcome of cytotoxic gene therapy of cancer. Here, we showed that the

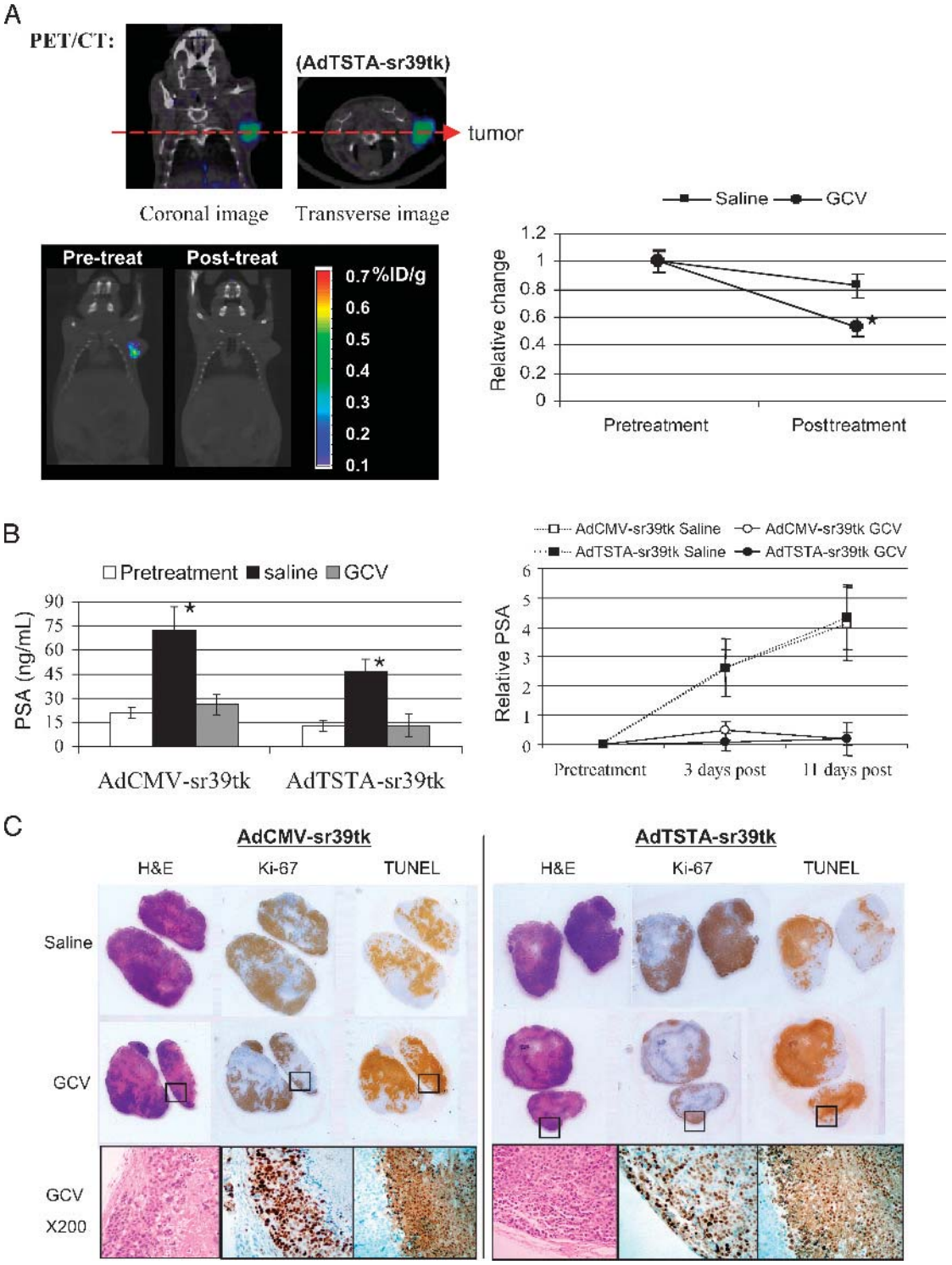

Figure 4. *Therapeutic effects of GCV treatment on the tumors. (A) PET signal in AdTSTA-sr39tk injected mice. The close-up coronal and transverse images represent a PET/CT study performed on an animal 8 days after intratumoral injection of AdTSTA-sr39tk. The lower paired images are the PET/CT results of a representative animal pre- and posttreatment with GCV. The tumor localized PET signals declined post-GCV treatment. The graph on the right shows the relative change of PET signal in the tumors of the two cohorts. The difference in the signal decay between the saline and GCV groups was significant ($p = .029$). (B) Serial PSA levels. GCV treatment in the CMV and TSTA groups resulted in a significant decrease in the serum PSA level compared with saline controls ($p = .02$). Relative change of PSA showed that the rate of the rising level was halted by GCV treatment. (C) Detailed tumor histology. Two representative tumors were shown for each condition under unmagnified objective. Consecutive thin sections were stained with hematoxylin and eosin (H & E), anti-Ki67 antibody (cell proliferation marker), and TUNEL. Comparing the lower panels of GCV-treated tumors to the upper saline controls; drug treatment resulted in decreased nucleated cells (blue staining on H&E), reduced proliferating cells (Ki-67), and elevated apoptosis (TUNEL). Higher magnification of the sections (×200) demonstrates specificity of the staining.*

adenovirus-based TSTA system can express the suicide gene in a robust, tissue-specific manner. The tissue selectivity of the TSTA method restricted the transgene expression to the LAPC-4 human prostate tumor, and thus, limited the transgene-mediated toxicity in a nontargeted organ such as the liver. The highly augmented activity of TSTA allowed the visualization of transgene expression by bioluminescent and PET imaging during treatment.

We postulated that functional gene expression activity in the tumor might provide more accurate, dynamic information on the content of living cells in a tumor than tumor size measurements. Due to its easy-to-use and rapid scan time capabilities, in vivo optical imaging has been applied frequently to interrogate tumor activities [13,14,16–22], including monitoring growth and therapy of marked tumors [22]. However, when we applied optical imaging to monitor the therapeutic effects of suicide gene therapy on renilla luciferase-labeled LAPC-4 tumors, changes in intratumoral signals were not correlated with treatment effects. Several factors could contribute to the difficulties we encountered. (i) Optical signal is known to be attenuated by hemoglobin levels, extent of tissue depth or necrotic tissue, and (ii) high, saturated signals in the xenograft tumors could make lost of signal during therapy difficult to detect. Thus, we decided to utilize PET imaging, which is a high-energy modality that is not attenuated by tissue depth, and it is applicable to human subjects. In fact, [^{18}F]FHBG was determined to be a safe tracer in healthy human volunteers [34]. Our results support the use of PET/CT to monitor the pharmacokinetic of HSV-tk suicide gene therapy in vivo.

Despite substantial tumor destruction in the suicide gene treatment, the tumor cell annihilation was incomplete at the specified end point of this study (Day 22). Potentially, a more prolonged treatment course could achieve more extensive tumoricidal effects. To ensure accuracy of gene delivery, we intentionally employed large size tumors, ~0.8cm diameter at the start of therapy. Consequently, one limiting factor likely to have contributed is the incomplete gene transduction via intratumoral viral injection. Several measures were attempted to achieve more optimal intratumoral transduction. To circumvent the high intratumoral pressure, the viral solution was administrated at a slow rate, in a small volume, divided into multiple sites and over several days. Despite these measures, the transduction rate was between 30% and 50%, which was estimated by performing flow cytometry of single-cell suspension of tumors 4 days after injection of a viral vector expressing green fluorescent protein (data not shown). Several strategies can be applied to enhance therapeutic efficacy of suicide gene therapy. The high level and specific gene expression accomplished by the TSTA method is helpful to maximize in vivo gene transduction as well as to boost the bystander effect. This bystander phenomenon, where cytotoxic effect spreads from transduced cells to neighboring nontransduced cells, is known to be augmented by increasing intercellular transfer of metabolites through gap junctions [35,36]. By combining the HSV-tk cytotoxic approach with other gene-based therapeutic targets such as anti-angiogenic or immune activation strategies, synergistic enhancement of remedial effects could be accomplished. In the context of improving efficacy of cancer treatment, gene therapy should be considered as one arm of a multiprong approach to manage cancer. Thus, it is promising that adenoviral-mediated suicide gene therapy has been shown to induce radiation sensitizing effects in tumors [37].

Another interesting finding from this and other studies [8,16,38] is that intratumoral injections of viral vectors often result in ''leakage'' into the systemic circulation, triggering transgene expression in the liver. Ongoing research in our laboratory indicates that tumor models exhibit differential viral ''leakage'' [16], and this phenomenon is likely modulated by tumor vasculature. Hence, these findings further underscore the importance of incorporating a noninvasive mean to monitor the location of toxic transgene expression in vivo, thereby obtaining the assurance that the ''on-target'' and ''off-target'' effects can be visualized. One unanticipated finding is that higher PET signal was detected in the liver of the AdCMV-sr39tk injected animal despite a much higher level of sr39tk gene delivery to the tumor (Figure 3). The possible explanations could be: (i) preferential adenoviral transduction of hepatocytes or (ii) preferential gene expression mediated by the CMV promoter in the liver or (iii) limiting PET substrate delivery to the tumor relative to the liver. We are actively investigating these possibilities.

In an attempt to improve prostate cancer gene therapy, we have coupled noninvasive imaging to a highly amplified, prostate tissue-specific gene expression system to express an enhanced cytotoxic HSV1-tk gene (sr39tk). The results demonstrated here confirm that the adenoviral vector containing prostate-specific TSTA system can achieve targeted expression in vivo. In the delivery of the potent variant sr39tk gene, effective tumor eradication with minimal systemic toxic affects was achieved. The coupling of PET imaging to this targeted suicide gene therapy will be a promising strat-

egy to develop future clinical protocols for patients with advanced stage prostate cancer.

Acknowledgments

Without the imaging technology infrastructure developed by Dr. Michael Phelps (Molecular and Medical Pharmacology, School of Medicine, UCLA) and the UCLA Crump Institute for Biological Imaging, this work could not be accomplished. We thank Waldemar Ladno, Judy Edwards, David Stout for their skillful assistance in PET/CT imaging, and Baohui Zhang for technical assistance. We deeply appreciate the guidance and shared equipment provided by Vivek Dixit (Department of Medicine, School of Medicine, UCLA) in the liver enzyme assay, and Giri Sulur for manuscript preparation. We thank Drs. Elizabeth Neufeld and Harvey Herschman for their helpful inputs. This work is supported by the California Cancer Research Program 3NI0226 (to LW), DAMD17-03-1-0095 (to LW), NIH R01 CA101904 (to LW), and an interdisciplinary seed grant from the JCCC (to MC, LW, and SSG). MS is supported by a DOD CDMRP postdoctoral fellowship (PC020531).

References

[1] Kasamon KM, Dawson NA (2004). Update on hormone-refractory prostate cancer. *Curr Opin Urol.* **14:**185–193.

[2] Stroh C, Held J, Samraj AK, Schulze-Osthoff K (2003). Specific inhibition of transcription factor NF-kappaB through intracellular protein delivery of I kappaBalpha by the Herpes virus protein VP22. *Oncogene.* **22:**5367–5373.

[3] Stacpoole PW, Owen R, Flotte TR (2003). The pyruvate dehydrogenase complex as a target for gene therapy. *Curr Gene Ther.* **3:**239–245.

[4] Herrmann F (1995). Cancer gene therapy: Principles, problems, and perspectives. *J Mol Med.* **73:**157–163.

[5] Qiao J, Doubrovin M, Sauter BV, Huang Y, Guo ZS, Balatoni J, Akhurst T, Blasberg RG, Tjuvajev JG, Chen SH, Woo SL (2002). Tumor-specific transcriptional targeting of suicide gene therapy. *Gene Ther.* **9:**168–175.

[6] Kubo H, Gardner TA, Wada Y, Koeneman KS, Gotoh A, Yang L, Kao C, Lim SD, Amin MB, Yang H, Black ME, Matsubara S, Nakagawa M, Gillenwater JY, Zhau HE, Chung LW (2003). Phase I dose escalation clinical trial of adenovirus vector carrying osteocalcin promoter-driven herpes simplex virus thymidine kinase in localized and metastatic hormone-refractory prostate cancer. *Hum Gene Ther.* **14:**227–241.

[7] Shalev M, Kadmon D, Teh BS, Butler EB, Aguilar-Cordova E, Thompson TC, Herman JR, Adler HL, Scardino PT, Miles BJ (2000). Suicide gene therapy toxicity after multiple and repeat injections in patients with localized prostate cancer. *J Urol.* **163:**1747–1750.

[8] Somia N, Verma IM (2000). Gene therapy: Trials and tribulations. *Nat Rev Genet.* **1:**91–99.

[9] Adams JY, Johnson M, Sato M, Berger F, Gambhir SS, Carey M, Iruela-Arispe ML, Wu L (2002). Visualization of advanced human prostate cancer lesions in living mice by a targeted gene transfer vector and optical imaging. *Nat Med.* **8:**891–897.

[10] Wu L, Sato M (2003). Integrated, molecular engineering approaches to develop prostate cancer gene therapy. *Curr Gene Ther.* **3:**452–467.

[11] Latham JP, Searle PF, Mautner V, James ND (2000). Prostate-specific antigen promoter/enhancer driven gene therapy for prostate cancer: Construction and testing of a tissue-specific adenovirus vector. *Cancer Res.* **60:**334–341.

[12] Wu L, Matherly J, Smallwood A, Adams JY, Billick E, Belldegrun A, Carey M (2001). Chimeric PSA enhancers exhibit augmented activity in prostate cancer gene therapy vectors. *Gene Ther.* **8:** 1416–1426.

[13] Zhang L, Adams JY, Billick E, Ilagan R, Iyer M, Le K, Smallwood A, Gambhir SS, Carey M, Wu L (2002). Molecular engineering of a two-step transcription amplification (TSTA) system for transgene delivery in prostate cancer. *Mol Ther.* **5:**223–232.

[14] Iyer M, Wu L, Carey M, Wang Y, Smallwood A, Gambhir SS (2001). Two-step transcriptional amplification as a method for imaging reporter gene expression using weak promoters. *Proc Natl Acad Sci USA.* **98:**14595–14600.

[15] Pantuck AJ, Matherly J, Zisman A, Nguyen D, Berger F, Gambhir SS, Black ME, Belldegrun A, Wu L (2002). Optimizing prostate cancer suicide gene therapy using herpes simplex virus thymidine kinase active site variants. *Hum Gene Ther.* **13:** 777–789.

[16] Sato M, Johnson M, Zhang L, Zhang B, Le K, Gambhir SS, Carey M, Wu L (2003). Optimization of adenoviral vectors to direct highly amplified prostate-specific expression for imaging and gene therapy. *Mol Ther.* **8:**726–737.

[17] Zhang L, Johnson M, Le KH, Sato M, Ilagan R, Iyer M, Gambhir SS, Wu L, Carey M (2003). Interrogating androgen receptor function in recurrent prostate cancer. *Cancer Res.* **63:** 4552–4560.

[18] Ray P, Bauer E, Iyer M, Barrio JR, Satyamurthy N, Phelps ME, Herschman HR, Gambhir SS (2001). Monitoring gene therapy with reporter gene imaging. *Semin Nucl Med.* **31:**312–320.

[19] Bhaumik S, Gambhir SS (2002). Optical imaging of Renilla luciferase reporter gene expression in living mice. *Proc Natl Acad Sci USA.* **99:**377–382.

[20] Contag PR, Olomu IN, Stevenson DK, Contag CH (1998). Bioluminescent indicators in living mammals. *Nat Med.* **4:**245–247.

[21] Wu JC, Sundaresan G, Iyer M, Gambhir SS (2001). Noninvasive optical imaging of firefly luciferase reporter gene expression in skeletal muscles of living mice. *Mol Ther.* **4:**297–306.

[22] Rehemtulla A, Stegman LD, Cardozo SJ, Gupta S, Hall DE, Contag CH, Ross BD (2000). Rapid and quantitative assessment of cancer treatment response using in vivo bioluminescence imaging. *Neoplasia.* **2:**491–495.

[23] Kokoris MS, Black ME (2002). Characterization of herpes simplex virus type 1 thymidine kinase mutants engineered for improved ganciclovir or acyclovir activity. *Protein Sci.* **11:** 2267–2272.

[24] Gambhir SS, Bauer E, Black ME, Liang Q, Kokoris MS, Barrio JR, Iyer M, Namavari M, Phelps ME, Herschman HR (2000). A mutant herpes simplex virus type 1 thymidine kinase reporter gene shows improved sensitivity for imaging reporter gene expression with positron emission tomography. *Proc Natl Acad Sci USA.* **97:**2785–2790.

[25] Nasu Y, Kusaka N, Saika T, Tsushima T, Kumon H (2000). Suicide gene therapy for urogenital cancer: Current outcome and prospects. *Mol Urol.* **4:**67–71.

[26] Wiewrodt R, Amin K, Kiefer M, Jovanovic VP, Kapoor V, Force S, Chang M, Lanuti M, Black ME, Kaiser LR, Albelda SM (2003). Adenovirus-mediated gene transfer of enhanced Herpes simplex virus thymidine kinase mutants improves prodrug-mediated tumor cell killing. *Cancer Gene Ther.* **10:**353–364.

[27] He TC, Zhou S, da Costa LT, Yu J, Kinzler KW, Vogelstein B (1998). A simplified system for generating recombinant adenoviruses. *Proc Natl Acad Sci USA.* **95:**2509–2514.

[28] Sato M, Johnson M, Zhang L, Gambhir SS, Carey M, Wu L (in press). Functionality of androgen receptor-based gene ex-

pression imaging in hormone refractory prostate cancer. *Clin Cancer Res.*

[29] Klein KA, Reiter RE, Redula J, Moradi H, Zhu XL, Brothman AR, Lamb DJ, Marcelli M, Belldegrun A, Witte ON, Sawyers CL (1997). Progression of metastatic human prostate cancer to androgen independence in immunodeficient SCID mice. *Nat Med.* **3:** 402–408.

[30] Townsend DW, Carney JP, Yap JT, Hall NC (2004). PET/CT today and tomorrow. *J Nucl Med.* **45:**4S–14S.

[31] Craft N, Chhor C, Tran C, Belldegrun A, DeKernion J, Witte ON, Said J, Reiter RE, Sawyers CL (1999). Evidence for clonal outgrowth of androgen-independent prostate cancer cells from androgen-dependent tumors through a two-step process. *Cancer Res.* **59:**5030–5036.

[32] Craft N, Shostak Y, Carey M, Sawyers CL (1999). A mechanism for hormone-independent prostate cancer through modulation of androgen receptor signaling by the HER-2/neu tyrosine kinase. *Nat Med.* **5:**280–285.

[33] Chen CD, Welsbie DS, Tran C, Baek SH, Chen R, Vessella R, Rosenfeld MG, Sawyers CL (2004). Molecular determinants of resistance to antiandrogen therapy. *Nat Med.* **10:**33–39.

[34] Yaghoubi S, Barrio JR, Dahlbom M, Iyer M, Namavari M, Satyamurthy N, Goldman R, Herschman HR, Phelps ME, Gambhir SS (2001). Human pharmacokinetic and dosimetry studies of [(^{18})F]FHBG: A reporter probe for imaging herpes simplex virus type-1 thymidine kinase reporter gene expression. *J Nucl Med.* **42:**1225–1234.

[35] Fick J, Barker FG 2nd, Dazin P, Westphale EM, Beyer EC, Israel MA (1995). The extent of heterocellular communication mediated by gap junctions is predictive of bystander tumor cytotoxicity in vitro. *Proc Natl Acad Sci USA.* **92:**11071–11075.

[36] Mesnil M, Yamasaki H (2000). Bystander effect in herpes simplex virus-thymidine kinase/ganciclovir cancer gene therapy: Role of gap-junctional intercellular communication. *Cancer Res.* **60:** 3989–3999.

[37] Rogulski KR, Zhang K, Kolozsvary A, Kim JH, Freytag SO (1997). Pronounced antitumor effects and tumor radiosensitization of double suicide gene therapy. *Clin Cancer Res.* **3:**2081–2088.

[38] Lohr F, Huang Q, Hu K, Dewhirst MW, Li CY (2001). Systemic vector leakage and transgene expression by intratumorally injected recombinant adenovirus vectors. *Clin Cancer Res.* **7:** 3625–3628.